Control of adipose tissue inflammation by hypothalamic SF1 neurons

Rashid, Misbah

The Graduate University for Advanced Studies,

SOKENDAI

School of Life Science

Department of Physiological Sciences

Table of Contents

Abstract

In obesity, excessive fat storage results in dysfunctional adipose tissue, which is accompanied by adipose tissue inflammation that is characterized by macrophage infiltration and pro-inflammatory cytokines production. Steroidogenic factor 1-expressing neurons (SF1 neurons) in the ventromedial hypothalamus (VMH) play an essential role in controlling energy metabolisms of peripheral tissues, including brown adipose tissue (BAT) and white adipose tissue (WAT). However, whether SF1 neurons regulate obesity-induced inflammatory responses in adipose tissue is unknown. In the current study, I investigated the roles of SF1 neurons on inflammatory responses in adipose tissue of high-fat diet-fed obese mice. Ablation of SF1 neurons by specific expression of diphtheria toxin-A (DTA) resulted in increased body weight, decreased energy expenditure, and impaired glucose and lipid metabolisms. Notably, ablation of SF1 neurons aggravated the obesity-induced inflammatory responses in the inguinal WAT (ingWAT) and impaired thermogenic activity in BAT whereas epididymal WAT (epiWAT) remained unaffected. In contrast, chronic stimulation of SF1 neurons by the use of a chemogenetic method ameliorated such inflammatory responses in ingWAT and upregulated thermogenic genes in BAT. These findings demonstrate that SF1 neurons mitigate obesity-induced inflammatory responses differently in various adipose tissue depots, and provide the first evidence to reveal a connection between the VMH and inflammatory responses in adipose tissues.

Abbreviations

AAV	Adeno-associated virus
AD4BP	Adrenal 4 binding protein
ANOVA	Analysis of variance
AP	Anteroposterior
ATMs	Adipose tissue macrophages
β2-AR	Beta-2 adrenergic receptor
BAT	Brown adipose tissue
BSA	Bovine serum albumin
CytC	Cytochrome C
CNO	Clozapine N-oxide
CNS	Central nervous system
cDNA	Complementary deoxyribonucleic acid
CPT1b	Carnitine palmitoyltransferase 1b
DTA	Diphtheria toxin-A
DREADD	Designer receptors exclusively activated by designer drugs
DV	Dorsoventral
DCM	Dichloromethane
DEG	Differentially expressed genes
DIO2	Iodothyronine deiodinase
GTT	Glucose tolerance test
GO	Gene ontology
GastroR	Red part of gastrocnemius

GastroW	White part of gastrocnemius
HFD	High-fat diet
IL-6	Interleukin-6
ingWAT	Inguinal white adipose tissue
ITT	Insulin tolerance test
MCP-1	Monocyte chemoattractant protein-1
ML	Mediolateral
NR5A1	Nuclear receptor subfamily 5 group A member 1
ND	Normal diet
OCT	Optimal cutting temperature
PFA	Paraformaldehyde
PBS	Phosphate-buffered saline
PGC-1α	Peroxisome proliferator-activated receptor gamma coactivator-1 alpha
RQ	Respiratory quotient
RT	Room temperature
RFP	Red fluorescent protein
RNA-seq	RNA sequencing
RT-PCR	Reverse transcription-polymerase chain reaction
RT-qPCR	Real time-quantitative polymerase chain reaction
RYR2	Ryanodine receptor 2
SF1	Steroidogenic factor 1
SNS	Sympathetic nervous system
SD	Standard deviation
SERCA2b	Sarcoplasmic/endoplasmic reticulum calcium ATPase 2b
TNF-α	Tumor necrosis factor-alpha

Tg	Transgenic
TPM	Transcripts per million
TFAM	Mitochondrial transcriptional factor A
UCP1	Uncoupling protein1
VO_2	Volume of oxygen consumption
VCO_2	Volume of carbon dioxide production
VMH	Ventromedial hypothalamus
WT	Wild type

Introduction

In response to challenges from the external or internal environment, our bodies have a mechanism called "homeostasis" that maintains a stable internal state. Energy homeostasis involves the balance between production/storage and consumption/utilization of energetic substances and is strictly regulated to keep the amount of energy in the body within a certain range. Disruption of energy homeostasis by excessive energy intake or decrease of energy utilization leads to metabolic diseases such as diabetes and obesity. Obesity is a complex disorder that is strongly linked to a sedentary lifestyle and insufficient physical activity. When total energy intake exceeds total energy expenditure, body weight increases, and then it causes many metabolic diseases, including cardiovascular disease, non-alcoholic fatty liver disease, and type 2 diabetes mellitus[1].

The central nervous system (CNS) plays an important role in the regulation of energy balance. The CNS receives and integrates internal and external information about energy and nutrients, and coordinates energy metabolism of peripheral tissues. In particular, the hypothalamus, which is located in the deepest part of the brain, regulates systemic energy metabolism, which includes feeding behavior and energy consumption[2,3]. It has become evident that abnormal neural activity in some hypothalamic neurons is closely associated with overeating and abnormal glucose and lipid metabolism, which leads to obesity, diabetes, and other metabolic disorders[4].

The ventromedial hypothalamus (VMH) is one of the important hypothalamic nuclei controlling energy homeostasis. Previous numerous studies highlighted the role of the VMH in the regulation of body weight and energy metabolism. Several studies with the VMH lesion revealed hyperphagia and obesity in animals[5–8], while electrical stimulation of the VMH was found to increase glucose production in the liver, lipolysis in adipose tissue, and glucose uptake

in some peripheral tissues such as brown adipose tissue (BAT) and skeletal muscles[9–13]. Injection of adipocyte hormone, leptin, into the VMH also increased glucose uptake in BAT, heart, and skeletal muscles[14,15]. Furthermore, leptin injection into the medial hypothalamus including the VMH increased fatty acid oxidation in skeletal muscles[16]. Orexin is also reported to stimulate glucose uptake in skeletal muscles via the VMH neurons[17]. Electrolytic VMH ablation could led to a further increase in body weight even in rats who were already obese when fed a high-fat diet (HFD)[18]. Thus, the role of the VMH is implicated in the modulation of energy expenditure and glucose and lipid metabolisms.

The VMH is comprised of a diverse group of neurons[19–21]. The dorsomedial part of the VMH is the brain region that exclusively contain neurons expressing the steroidogenic factor 1 (SF1) (also called AD4BP and Nr5a1) in the CNS[22]. SF1 is a transcription factor found in steroidogenic tissues such as the adrenal gland and gonads, but its expression in the brain is limited to the pituitary gland and the VMH[23]. Homozygous deletion of SF1 resulted in an abnormal VMH growth, implying that SF1 plays an important role in the VMH development[24–26]. Optogenetic stimulation of SF1 neurons induced hyperglycemia and enhanced the counterregulatory response to hypoglycemia, whereas photoinhibition of SF1 neurons disrupts recovery from insulin-induced hypoglycemia[27]. Acute chemogenetic activation of SF1 neurons increased energy expenditure and whole-body glucose utilization by increasing glucose uptake in certain peripheral tissues including BAT, heart and skeletal muscles, and glucose production in the liver, thereby maintaining the normal blood glucose levels[28]. The deletion of the leptin receptor in SF1 neurons of the VMH resulted in increased body weight and energy intake, and impaired glucose homeostasis[29,30]. Genetic disruption of vesicular glutamate transporter 2, insulin receptor, phosphoinositide 3-kinase, protein tyrosine phosphatase 1B, and AMP-activated protein kinase $\alpha 1$ subunit in SF1 neurons altered glucose, lipid, and energy

metabolism in mice[31–35]. All of the studies pointed to the important roles of SF1 neurons in the regulation of body weight and energy metabolism.

While increased food intake/body weight and impaired energy/glucose metabolisms are prominent factors of obesity, one of the essential components of obesity is impaired adipose tissue function. Adipose tissues, especially white adipose tissue, are not only the energy storage organ but also an essential endocrine organ which is one of the main sources of endocrine signals (adipokine) for energy metabolism, such as leptin and adiponectin[36]. Increased adiposity in obesity results in an impaired adipose tissue function, which is accompanied by adipose tissue inflammation[37–40]. In adipose tissue of lean animals, anti-inflammatory polarization of macrophages, called M2 macrophages, are major adipose tissue macrophages (ATMs) that are involved in cell maintenance and repair. As adiposity increases, the increased size and number of adipocytes reduces vascular supply, and results in hypoxia and eventually, adipocyte death, which triggers recruitment of pro-inflammatory macrophages, called M1 macrophages that induces an excessive cytokine and chemokine secretion[41,42]. The number of M1 macrophages drastically increases by augmented infiltration and local proliferation and undergoes a significant change in distribution. These M1 polarized macrophages secrete a slew of inflammatory cytokines, including tumor necrosis factor-alpha (TNF-α), interleukin-6 (IL-6), and monocyte chemoattractant protein-1 (MCP-1)[43]. These cytokines released from ATMs interfere with insulin signaling, causing insulin resistance and the inflammatory responses in the periphery[44,45].

Accumulating evidence supports the idea that the CNS controls not only energy homeostasis but also immune homeostasis. Recent studies have identified specific brain areas that control humoral immune response or immunological host defense activities[46,47]. It has been shown that the central melanocortin system maintains an anti-inflammatory state in ATMs of lean mice in vivo via the sympathetic nervous system (SNS) and beta 2-adrenergic receptor

(β2-AR) pathway[48]. However, whether inflammatory responses in adipose tissues in HFD-induced obese animals are regulated by the CNS remains unclear.

In this study, I investigated the roles of SF1 neurons in the genes expression involved in inflammatory responses in adipose tissues in HFD-induced obese mice [hereafter called diet-induced obese (DIO) mice]. I specifically modulated SF1 neurons in the VMH and analyzed HFD-induced inflammatory responses in adipose tissues along with whole-body energy metabolism in mice. I ablated SF1 neurons by specific expression of diphtheria toxin-A (DTA) and activated SF1 neurons chronically via DREADD (designer receptors exclusively activated by designer drugs) system.

The ablation of SF1 neurons increased body weight, decreased energy expenditure and lipid oxidation, and impaired glucose metabolism in DIO mice. In SF1-ablated mice, genes expression for macrophage markers and inflammatory cytokines were increased in inguinal white adipose tissue (ingWAT) but not in epididymal white adipose tissue (epiWAT). The finding in ingWAT was confirmed by the immunohistochemical analysis and further supported by transcriptomic analysis of ingWAT of DIO mice. RNA sequencing (RNA-seq) analysis revealed that SF1 neuron ablation increases the expression of many inflammatory response-related genes in ingWAT. Furthermore, the ablation of SF1 neurons significantly decreased the expression of thermogenesis and mitochondria-related genes in BAT.

In contrast, chronic activation of SF1 neurons substantially suppressed the expression of inflammatory genes in ingWAT but not in epiWAT in DIO mice. It enhanced the expression of thermogenic genes in BAT. Importantly, the chronic activation of SF1 neurons decreased the inflammatory responses in ingWAT even in mice that had already developed diet-induced obesity before SF1 stimulation. These results, taken together, suggest that VMH SF1 neurons have an inhibitory role in inflammatory responses in ingWAT and a stimulatory role in

thermogenesis in BAT in DIO mice. This study provides the first evidence of a crucial link between the VMH and inflammatory responses in ingWAT.

Materials and Methods

Animals

Transgenic mice expressing Cre-recombinase in the SF1 neurons (SF1-Cre)[29] were purchased from the Jackson laboratory [STOCK Tg (Nr5a1-cre)7Lowl/J]. Hemizygous SF1-Cre mice were bred with FVB/N mice (Clea, Tokyo, Japan) or C57BL/6J mice (SLC, Hamamatsu, Japan). All mice were fed with a laboratory chow diet (CE-2) (Clea, Tokyo, Japan) otherwise noted, and were maintained at a constant temperature at 24 ± 2°C with a 12-hour light-dark period. Eight to 47-week-old male mice housed individually were used in all experiments. All experimental procedures were carried out in compliance with institutional guidelines for the care and handling experimental animals and were authorized by Institutional Animal Care and Use Committee of National Institutes of Natural Sciences.

Viral Injection

Mice were anesthetized with an intraperitoneal injection of a mixture of ketamine (100 mg/kg) and xylazine (10 mg/kg). The skulls of anesthetized mice were fixed to the stereotaxic frame, and 32G needles with Hamilton Neurosyringe (Hamilton, Reno NV, USA) loaded with viruses were inserted into the VMH. The stereotaxic coordinates for the VMH injections were determined relative to Bregma obtained from the atlas by Franklin and Paxinos[49]. The coordinates used for targeting the VMH were - 1.30 mm (anteroposterior, AP), ± 0.04 mm (mediolateral, ML), - 5.50 mm (dorsoventral, DV). To ablate SF1 neurons, 400 nl of adeno-associated virus (AAV) coding AAV-EF1a-mCherry-FLEX-DTA (3.7×10^{12} viral particles/ml, UNC vector core, Chapel Hill NC, USA) was injected into both sides of the VMH in SF1-Cre mice or wildtype (WT) siblings. To activate SF1 neurons, 300nl of AAV-hSyn-DIO-hM3Dq-mCherry (2.2×10^{13} viral particles/ml, Addgene, Watertown MA, USA) was injected into both

sides of the VMH in SF1-Cre mice (SF1-stimulated mice). As this control, the same volume of AAV-hSyn-DIO-mCherry (2.6 x 10^{13} viral particles/ml, Addgene) was injected into both sides of the VMH in SF1-Cre mice (control mice). After virus injection, mice were subcutaneously injected analgesic buprenorphine (0.05 mg/kg) (Otsuka Pharmaceutical, Tokyo, Japan) and applied a drop of local analgesia (lidocaine, Aspen, Tokyo, Japan) on the wound, and skin was sutured. To avoid infection, mice were given an antibiotic ointment around the wound and were monitored for a few days.

Animal Treatment

Ablation of SF1 neurons

Mice were given 5 weeks of recovery with free access to laboratory chow and water after receiving AAV-FLEX-DTA injections into SF1-Cre and WT mice. Mice were then fed with HFD [60% kcal from fat, 20% kcal from carbohydrate, and 20% kcal from protein (D12492, Research Diets, Brunswick NJ, USA)] for 8 weeks. Total calorie intake was calculated as follows; Total food intake (g) x 5.24 kcal/g. In this experiment, mice were placed in special cages to measure energy expenditure via indirect calorimetry system (see below). Following that, mice were subjected to glucose and insulin tolerance tests (GTT and ITT) while on HFD (see below).

Stimulation of SF1 neurons

After 2 weeks of recovery from a viral infection, SF1-Cre mice injected with AAV expressing mCherry-fused hM3Dq (hM3Dq-mCherry) or only mCherry in the VMH were fed with HFD for 4 weeks. Five mg/kg BW per day of clozapine-N-oxide (CNO, Cayman, Ann Arbor MI, USA) were added into the drinking water to activate hM3Dq along with HFD feeding. In another experiment, SF1-Cre mice injected with AAV expressing hM3Dq-mCherry in the VMH were fed with HFD for 8 weeks and CNO or saline was then added to the drinking water

for the next 4 weeks with continued HFD feeding. Obese mice that gained more than 30% of their body weight after 8 weeks on the HFD were randomly provided with either CNO or saline.

Indirect Calorimetry

The energy expenditure and respiratory quotient (RQ) were determined using indirect calorimetry system. Oxygen consumption (VO_2) and carbon dioxide production (VCO_2) from each mouse were measured by a mass spectrometric analyzer (Arco-2000; Arco System, Chiba, Japan). To measure locomotor activity, a force plate system (Actracer-2000; Arco System) was mounted beneath the cage to detect low-intensity movements.

The VO_2 and VCO_2, as well as locomotor activity, were simultaneously measured every 10 minutes for 2 days after 2 days of acclimation. Total energy expenditure and the amount of oxidized fat and carbohydrate were calculated from VO_2 and VCO_2 as mentioned previously[50] by the following equations;

Energy expenditure (kcal/min) = $(3.816 \times VO_2) + (1.231 \times VCO_2)/1000$

Fat oxidation (kcal/min) = $(1.67 \times [VO_2 - VCO_2]) \times 9.3/1000$

Carbohydrate oxidation (kcal/min) = $([4.51 \times VCO_2] - [3.18 \times VO_2]) \times 4.1/1000$

Basal energy expenditure (cal/min) was calculated with logarithmically converted locomotor activity ($\log_{10}$ (activity + 1) on the x-axis and energy expenditure (cal/min) per mouse on the y-axis. Y-intercept on the y-axis of the linear regression was determined as the basal energy expenditure.

Glucose & Insulin Tolerance Test

For glucose tolerance test (GTT), mice were fasted for 16 hours and then intraperitoneally injected glucose dissolved in saline (1 g/kg BW). Blood was obtained from the tail vein by small incision with a scalpel and blood glucose concentrations were measured with a Lab Gluco glucometer (ForaCare, Moorpark, CA, USA). Glucose concentrations were measured at 0

(before glucose administration) and 15, 30, 60, 90, and 120 minutes after glucose administration.

For insulin tolerance test (ITT), mice were fasted for 3 hours and then intraperitoneally injected insulin (Sigma-Aldrich Japan, Tokyo, Japan) dissolved in saline (0.5 U/kg BW). Blood glucose concentrations were measured with a Lab Gluco glucometer at 0 (before insulin administration) and 15, 30, 60, and 90 minutes after insulin administration.

Tissue Collection

Mice were fasted for 3 hours during the light period. Mice were then euthanized by cervical dislocation and blood samples were collected from the heart by making an incision. Plasma samples were obtained by centrifuging the blood at 1200 x g for 15 minutes in heparin-added tubes and aliquots of plasma samples were used for the measurement of plasma insulin concentrations. Brains and peripheral tissues (ingWAT, epiWAT, interscapular BAT, heart, liver, pancreas, soleus, red and white parts of gastrocnemius) were collected and the weight of peripheral tissues was measured. Brains and a part of ingWAT were fixed in the 4% paraformaldehyde (PFA) solution. Other parts of tissues and plasma samples were quickly frozen in liquid nitrogen. Frozen tissues were preserved at -80^{o}C until analysis.

Plasma Insulin Measurement

Plasma concentrations of insulin were measured by insulin ELISA kit (Fujifilm WAKO, # 634-01481, Osaka, Japan) according to the manufacturer's instruction.

Immunohistochemistry

Brains

The brains were fixed in 4% PFA, soaked in 30% sucrose until the brains sunk, and then frozen in an optimal cutting temperature (OCT) compound (Sakura Finetek, Tokyo, Japan) mixed with 30% sucrose at a ratio of 2:1. Tissue blocks were cut into 20 μm thick sections using a cryostat (Frigocut 2800, Leica biosystems, Nussloch, Germany) mounted on glass slides and

stored at -20°C. Frozen slides were returned to room temperature (RT) and washed with phosphate-buffered saline (PBS) twice. Sections were incubated with 0.5% Triton X-100 in PBS and TNT (0.1 M Tris pH 7.5, 150 mM NaCl, 0.05% Tween) for 5 minutes. Then the slides were incubated overnight at 4°C with primary antibodies [rabbit anti-c-Fos (1:500 dilution; Cell Signaling #2250, Danvers MA, USA), goat anti-RFP (1:1000 dilution; Rockland #200-101-379, Pottstown PA, USA), and/or rabbit anti-SF1 (1:400 dilution; Millipore #07-618, Burlington MA, USA) antibodies] diluted in TNB (0.5% blocking reagent (Perkin Elmer # FP1012/1020, Waltham MA, USA) dissolved in TNT) or DSB (1% bovine serum albumin (BSA), 5% normal donkey serum dissolved in TNT). After washing three times in TNT, slides were incubated for 1 hour at RT with secondary antibodies [Alexa 488 or Alexa 568-labeled donkey antibodies against rabbit and/or goat immunoglobulin G (1:500 dilution; ThermoFisher, Waltham MA, USA)] and 0.5 μg/ml Hoechst33342 (ThermoFisher). All the slides were then coverslipped with Fluoromount-G (Southern Biotech, Birmingham AL, USA). For immunostaining for SF1 cells, an antigen retrieval method (incubation with boiled 10 mM citric acid buffer (pH 6.0) for 15 minutes with microwave) was used in place of 0.5% Triton X-100 in PBS incubation.

Adipose tissues

IngWAT was fixed in 4% PFA and delipidated as described previously[51]. Tissues were washed twice with PBS and dehydrated using methanol ascending gradients prepared in B1n buffer (20%, 40%, 60%, 80%, 100%) [B1n buffer: 0.3 M glycine, 0.1% Triton X-100]. IngWAT was delipidated by immersing in 100% dichloromethane (DCM) three times until the samples sunk. The tissues were washed twice with 100% methanol and rehydrated in a series of reversed methanol/B1n buffer gradients (80%, 60%, 40%, 20%, and 100% B1n buffer). The tissues were then washed with PBS and placed in 30% sucrose overnight. They were frozen in OCT and cut into 12-14 μm thick sections using a cryostat, mounted on glass slides, and stored at -20°C.

Slides were immunostained as described above with primary antibodies against macrophage markers [1:400 dilution; rat anti-F4/80 (Bio-Rad, #MCA497GA, Hercules CA, USA) or goat anti-CD206 (1:2000 dilution; R&D Systems, #AF2535, Minneapolis MN, USA) antibodies] and counterstained with Hoechst33342 (ThermoFisher) for nuclear staining.

Image Acquisition and Analysis

The images were obtained with a confocal microscope (FV3000, Olympus, Tokyo, Japan) by using FV31S-SW software. The brightness and contrast of the images were adjusted by using FIJI software (Version: 2.1.0/1.53c) as needed for visibility. The numbers of SF1 neurons and c-Fos-positive cells in the VMH were counted using FIJI software.

RNA Extraction and RT-qPCR

Total RNAs were extracted from frozen adipose tissues using Trizol reagent (ThermoFisher) and purified using RNA purification kit (PureLink RNA mini kit (ThermoFisher) or NucleoSpin RNA Kit (Takara, Shiga, Japan) and followed by RT-PCR (reverse transcription-polymerase chain reaction). The RNA samples (1 μg) were reverse transcribed using an oligo dT primer and ReverTra Ace reverse transcriptase (TOYOBO, Tokyo, Japan). The resulting cDNA was purified by a QIAquick PCR purification kit (Qiagen, Venlo, Netherland). Purified cDNA was used for RT-qPCR (real-time quantitative polymerase chain reaction) analysis by using Power SYBER green master mix (ThermoFisher) with StepOnePlus real-time PCR system (ThermoFisher). All mRNA expression data were normalized relative to the expression of 36B4. The primer sequences are shown in the table 1.

RNA-Seq Analysis

Total RNAs extracted from ingWAT as described above were used for RNA-seq analysis. The RNA-seq was performed by Eurofins Genomics Japan (Tokyo, Japan). Polyadenylated mRNAs were isolated, cDNAs were synthesized, and strand-specific mRNA libraries were generated. The generated library was sequenced by NovaSeq 6000 (Illumina, San Diego CA,

USA). First, fastq files were processed with an in-house NextFlow pipeline (github.com/palfalvi/rnaseq). Shortly, fastq files were fed to fastp v0.20.1 for quality assessment, adapter removal, and quality filtering[52]. Filtered reads were quantified using Kallisto v0.46.2 against the Mus musculus reference genome sequence (GRCm39 (mm39))[53]. Transcript abundances were read into R Statistical Software version 4.0.3 using the tximport package and quantifications of transcript levels were converted to the gene level[54]. Differentially expressed genes (DEGs) were identified with DESeq2 using Wald-test[55]. Gene Ontology (GO) enrichment analysis of selected genes sets was performed using the gage package[56]. To assess the changes in the expression of inflammatory genes by SF1 neuron ablation, DEGs with the following GO were analyzed. GO:0001816 cytokine production, GO:0002253 activation of the immune response, GO:0002252 immune effector process, GO:0002684 positive regulation of immune system process, GO:0006954 inflammatory response, GO:0034097 response to cytokine stimulus, GO:0045087 innate immune response, GO:0045321 leukocyte activation, GO:0050776 regulation of immune response, GO:0050778 positive regulation of immune response.

Statistical Analysis

The data are presented as means ± standard deviation (SD). Statistical analysis was performed with GraphPad Prism software (Version: 8.4.2 (464)). Multiple groups were compared using analysis of variance (ANOVA) followed by post hoc Sidak's test, while two groups were compared using unpaired *t*-test. qPCR data were analyzed after a logarithmic conversion. Statistical significance was determined by a *P* value less than 0.05.

Results

Preferential expression of DTA ablates SF1 neurons in the VMH in a Cre-dependent manner

To investigate the role of SF1 neurons in adipose tissue inflammation, I first ablated SF1 neurons from the VMH. I injected an AAV (AAV-EF1a-mCherry-FLEX-DTA, hereafter called AAV-FLEX-DTA) that expresses DTA in the presence of Cre-recombinase, while it expresses mCherry in the absence of Cre-recombinase, into the VMH of SF1-Cre mice. With this method, DTA expression is supposed to cause cell death only in SF1 neurons. Indeed, when AAV-FLEX-DTA was injected into the VMH of WT control mice, mCherry was expressed in and around the VMH (Fig. 1A). In contrast, when AAV-FLEX-DTA was injected into the VMH of SF1-Cre mice (hereafter the mice were called SF1-ablated mice), the number of mCherry and SF1-positive cells was significantly decreased in the VMH (Fig. 1B). The number of SF1 neurons in the VMH of SF1-ablated mice was about 3.5-fold less than that of WT control mice (Fig. 1C). These results indicated that AAV-FLEX-DTA injection effectively ablated SF1 neurons in the VMH in a Cre-dependent manner.

Ablation of SF1 neurons alters body weight and energy metabolism in DIO mice

To examine the effects of SF1 neuron ablation on body weight and energy metabolism in DIO mice, SF1-ablated and control mice were subjected to HFD feeding for 8 weeks after 5 weeks of recovery with normal diet (ND) feeding. SF1-ablated mice gained substantially more body weight than the control mice (Fig. 2A). The significant body weight gain was observed even during the recovery period but got more prominent during the HFD feeding period (Fig. 2B).

This rise in body weight was unrelated to food intake, as there was no change in food consumption (Fig. 2C, D).

I examined the effects of ablation of SF1 neurons on energy expenditure, locomotor activity, and RQ by using indirect calorimetry system. SF1-ablated mice significantly decreased oxygen consumption in both the light and dark periods and energy expenditure in the dark period (Fig. 3A, B), suggesting the important roles of SF1 neurons in the control of energy expenditure. Intriguingly, the increase in locomotor activity observed in WT control mice during the dark period was totally abolished in SF1-ablated mice (Fig. 3C). To examine the contribution of locomotor activity in energy expenditure in SF1-ablated mice, I calculated the basal energy expenditure of SF1-ablated and control mice by analyzing a Y axis-intersect in a linear regression between locomotor activity to the energy expenditure of individual mice (Fig. 3D, E). I found that the basal energy expenditure was significantly decreased in SF1-ablated mice compared with that in control mice (Fig. 3F). These results suggest that SF1 neuron ablation decreases basal energy expenditure as well as locomotor activity.

SF1-ablated mice increased RQ, which reflects the relative contributions of fat and carbohydrate oxidation on energy expenditure, during both light and dark periods (Fig. 3G). In accordance with the change in RQ, fat oxidation was reduced in SF1-ablated mice, though carbohydrate oxidation was unaffected (Fig. 3H, I). These results suggest that the ablation of SF1 neurons reduces energy expenditure and fat oxidation, which could contribute to body weight gain in SF1-ablated mice.

Ablation of SF1 neurons impairs glucose metabolism in DIO mice

To investigate the effects of ablation of SF1 neurons on glucose metabolism in DIO mice, I performed GTT in SF1-ablated and control mice. GTT showed that SF1-ablated mice significantly increased blood glucose levels compared with that of the control mice (Fig. 4A). Plasma insulin levels were not different between the two groups after 3 hours of fasting (Fig.

4B). I performed ITT to examine the insulin action on blood glucose concentration. Both groups showed a similar blood glucose reduction in response to insulin injection (0.5 mU/kg BW) (Fig. 4C).

Ablation of SF1 neurons alters the weight of peripheral tissues in DIO mice

I examined the weight of peripheral tissues in SF1-ablated and control mice (Fig. 5). Among tissues examined, the weight of ingWAT, heart, and liver were significantly increased in SF1-ablated mice (Fig. 5A, D, E). Interestingly, I found that the weight of epiWAT was decreased in SF1-ablated mice (Fig. 5C). Thus, white adipose tissues in distinct locations appear to be differently regulated by SF1 neurons in the VMH in DIO mice.

Ablation of SF1 neurons increases inflammatory responses in adipose tissues in DIO mice

To examine the effects of SF1 neuron ablation on inflammatory responses in adipose tissues in DIO mice, I analyzed the genes expression involved in inflammatory responses in the three types of adipose tissues, ingWAT, epiWAT, and BAT. I also analyzed the genes expression involved in energy expenditure to examine adipose tissue function. I compared the relative mRNA abundances between control and SF1-ablated mice. After 8 weeks of HFD feeding, SF1-ablated mice showed significantly higher mRNA levels of macrophage markers (F4/80, CD11c, and CD206) and inflammatory cytokine genes (TNF-α and MCP-1) than the control mice (Fig. 6A-F). In contrast, mRNA abundance of thermogenic or mitochondria-related genes remained unaltered in ingWAT (Fig. 6G-L). Immunohistochemical study showed the increased number of F4/80 or CD206 expressing cells in ingWAT of SF1-ablated mice (Fig. 7). Moreover, crown-like structures formed by macrophage aggregation surrounding adipocytes[57] were more frequently observed in ingWAT in the SF1-ablated mice than those in the control mice (Fig. 7). Similar to those in ingWAT, the mRNA abundances of macrophage markers (F4/80, CD11c, and CD206) were upregulated in BAT in SF1-ablated mice. However, the mRNA abundances

of inflammatory cytokines remained unchanged (Fig. 8A-F). Interestingly, in SF1-ablated mice, I found significantly lower expression of thermogenic markers (UCP1, PGC-1α, DIO2) in BAT, which are closely linked to the thermogenic activity (Fig. 8G-I). Moreover, the mRNA abundances of other mitochondrial genes (TFAM and CytC) and lipid oxidation gene (CPT1b) were substantially decreased (Fig. 8J-L), implying that thermogenic and mitochondrial functions are impaired in BAT in SF1-ablated mice. These findings thus suggest that the ablation of SF1 neurons causes an increase in macrophage accumulation and the impairment of thermogenic function in BAT.

In contrast to ingWAT and BAT, I found no change in the mRNA abundances of inflammatory response-related genes in epiWAT in SF1-ablated mice (Fig. 9A-F). Thermogenic and mitochondrial genes, except DIO2, remained unaltered as well (Fig. 9G-L). These results suggest that the genes expression of mitochondria and inflammatory responses in epiWAT are unaffected by the ablation of SF1 neurons in DIO mice.

To elucidate the molecular events after SF1 neuron ablation in ingWAT, I examined the comprehensive genes expression in ingWAT in SF-1 ablated mice using RNA-seq analysis. The analysis identified 752 upregulated and 1327 downregulated genes after SF1 neuron ablation among 17967 genes analyzed (Fig. 10A). Gene ontology enrichment analysis revealed that genes associated with immunological responses were highly enriched among genes upregulated in SF1-ablated mice (Fig. 10B). Fig.10C shows the upregulated genes annotated to inflammatory responses in ingWAT of SF1-ablated mice. Furthermore, RNA-seq analysis confirmed the results of qPCR in Fig. 6 for the mRNA abundances of macrophage markers (F4/80, CD11c, and CD206) and inflammatory cytokines (TNF-α and MCP-1) in SF1-ablated and control mice (Fig. 10D). These results suggest that inflammatory responses are the most affected biological events in ingWAT after SF1 neuron ablation in DIO mice. Together, these

results thus indicate that SF1 neurons play an important role in the regulation of inflammatory responses in ingWAT and BAT and thermogenic activity in BAT.

Activation of SF1 neurons in the VMH by DREADD technology

Exacerbation of inflammatory responses in adipose tissues after SF1 neuron ablation suggests that SF1 neurons in the VMH have an inhibitory role in inflammatory responses in ingWAT and BAT in DIO mice. To examine this possibility, I next investigated the effects of SF1 neuron activation on inflammatory responses in adipose tissues. I utilized a chemogenetic method DREADD: the hM3Dq-DREADD activates neurons through the Gq pathway in the presence of pharmacologically inert ligand CNO. I injected AAV that expresses mCherry alone (for control mice) or hM3Dq-mCherry (for SF1-stimulated mice) in a Cre-dependent manner into the VMH of SF1-Cre mice. Both groups of mice were fed with ND about 4 weeks, and CNO was administered through drinking water for one day. While mCherry was expressed in the neurons in the VMH in both control and SF1-stimulated mice (Fig. 11A, B), CNO administration only increased the number of neurons expressing c-Fos, a neuronal activation marker, in the VMH in the SF1-stimulated mice (Fig. 11C). This result indicates that oral administration of CNO activates SF1 neurons in the VMH.

Chronic activation of SF1 neurons has little effects on body weight, food consumption, and peripheral tissue weight in DIO mice

To investigate whether the chronic activation of SF1 neurons affects inflammatory responses in adipose tissues in DIO mice, both control and SF1-stimulated mice were fed with HFD along with CNO in a drinking water for 4 weeks. Although SF1-stimulated mice tended to gain less body weight, they revealed a similar body weight increase and food intake when compared with the control mice (Fig. 12). Similarly, SF1-activated mice did not show any difference in the weight of peripheral tissues, except BAT, from the control mice (Fig. 13).

Chronic activation of SF1 neurons suppresses inflammatory genes expression in adipose tissues in DIO mice

To examine the effects of chronic activation of SF1 neurons on inflammatory responses in adipose tissues during HFD feeding, I investigated inflammatory genes expression in ingWAT, BAT, and epiWAT. I found a significant reduction of mRNA abundances of macrophage markers (F4/80, CD206, and CD11c) and some inflammatory cytokines (IL-6 and MCP-1) in ingWAT of SF1-activated mice (Fig. 14A-F). Thus, chronic activation of SF1 neuron reduced some genes expression for inflammatory responses in ingWAT in HFD-fed mice. Unexpectedly, thermogenic genes (UCP1 and DIO2) decreased significantly upon the activation of the SF1 neurons, while mitochondria-related genes (PGC-1α, SERCA2b, and CPT1b) did not alter (Fig. 14G-J).

In BAT, the mRNA abundance of one macrophage marker (CD11c) significantly decreased after SF1 neuron activation (Fig. 15B), and F4/80 tended to be decreased (Fig. 15A), suggesting that chronic activation of SF1 neurons reduces the accumulation of inflammatory macrophages in BAT. However, the mRNA abundances of TNF-α, IL-6, and MCP-1 did not alter (Fig. 15D-F). Interestingly, the mRNA abundances of a thermogenic gene (UCP1) and mitochondria genes (CytC and CPT1b) were significantly increased in SF1-activated mice when compared with those in control mice (Fig. 15G, K, L). Similar to the results from SF1-ablated mice, the mRNA abundances of inflammatory responses and thermogenesis-related genes in epiWAT did not change after SF1 neuron activation (Fig. 16).

Taken together, these results suggest that, in contrast to the ablation of SF1 neuron, the activation of SF1 neuron suppresses the genes expression of inflammatory responses in ingWAT and BAT and upregulates the thermogenesis-related genes expression in BAT in HFD-fed mice. In contrast, SF1 neurons in the VMH unlikely regulate those genes expression in epiWAT in HFD-fed mice.

Chronic activation of SF1 neurons suppresses inflammatory genes expression in ingWAT in mice that developed obesity before neural stimulation

The above studies indicate that SF1 neurons regulate inflammatory genes expression in ingWAT in DIO mice. Ablation of SF1 neurons increased the mRNA abundances of macrophage markers and inflammation-related genes. In contrast, activation of SF1 neurons suppressed those genes expression. Therefore, I next examined whether the chronic activation of SF1 neurons suppresses HFD-induced inflammatory responses in ingWAT that are already developed in DIO mice before neuronal activation. For this purpose, mice expressing hM3Dq in SF1 neurons were fed with HFD without CNO administration for 8 weeks, and CNO or saline was administered through drinking water for the next 4 weeks with continued HFD feeding.

Both control and SF1-stimulated mice showed a similar increase in body weight before CNO treatment (Fig. 17A, B). CNO administration then tended to suppress the body weight gain of SF1-activated mice, but the body weight was comparable with the control mice on the sacrifice day (Fig. 17C). Food consumption did not alter before or after SF1 neuron activation (Fig. 17D, E). Hence, the chronic activation of SF1 neurons had only a small effect on body weight and food intake in DIO mice. Consistent with this, the weight of peripheral tissues examined, except that of the liver and red part of the gastrocnemius, did not show any differences between animals with and without CNO administration (Fig. 18). The activation of SF1 neurons significantly decreased the mRNA abundances of macrophage markers (F4/80, CD11c, and CD206) and inflammatory cytokines (IL-6 and MCP-1) in ingWAT which are already developed in DIO mice before SF1 neuron stimulation (Fig. 19A-F). The mRNA abundances of thermogenic genes in the ingWAT did not alter (Fig. 19G-I). These results

suggest that, even in mice that developed obesity before neural stimulation, chronic activation of SF1 neurons suppresses inflammatory responses in ingWAT.

Overall, my results have shown that VMH SF1 neurons have an inhibitory role in inflammatory responses in ingWAT and a stimulatory role in thermogenic function in BAT. However, it had little effect in epiWAT in DIO mice.

Discussion

Obesity is associated with the activation and release of harmful cytokines and chemokines that promote metabolic dysregulation. In the current study, I studied the roles of SF1 neurons in the VMH on HFD-induced obesity, especially on inflammatory responses in adipose tissues. I investigated the effects on HFD-induced inflammatory responses after the VMH-specific ablation of SF1 neurons using AAV that expresses DTA in a Cre-dependent manner. Furthermore, SF1 neurons in the VMH were activated by expressing DREADD receptor, hM3Dq, and the effects on inflammatory responses in adipose tissues were investigated. I demonstrate that ablation of SF1 neurons in the VMH aggravates the obesity-induced inflammatory responses in ingWAT and impairs thermogenic activity in BAT, whereas epiWAT remains unaffected. In contrast, chronic stimulation of the SF1 neurons ameliorates such inflammatory responses in ingWAT and upregulated thermogenic genes in BAT. These findings demonstrate that SF1 neurons in the VMH mitigate the DIO-induced inflammatory responses differently in various adipose tissues and provide the first evidence to reveal a connection between the VMH and inflammatory responses in adipose tissues.

I found that the VMH-specific SF1 neuron ablation led to metabolic complications during HFD feeding compared to control mice. These effects included increased body weight gain, decreased energy expenditure, and reduced glucose tolerance and lipid oxidation (Figs. 2-5). The rise in body weight gain was most likely to be due to a decline in energy expenditure because food intake was not different between the ablated and control groups (Fig. 2). Energy expenditure consists of basal energy expenditure and physical movements or exercise ("locomotor activity" in this study). Here, both basal energy expenditure and locomotor activity were significantly reduced after ablation of SF1 neurons in DIO mice (Fig. 3). A decrease in the basal energy expenditure could be a major contributing factor that decreased total energy

consumption in SF1-ablated mice (Fig. 3). Recently, a large number of studies have focused on the crucial role of adipose tissues in energy consumption. BAT contributes to the energy expenditure of small mammals and possibly humans by dissipating heat and can thus counteract weight gain[58–60]. IngWAT has been shown to be a potential thermogenic organ that contains "beige" fat cells[61–63]. The present studies suggest that ablation of SF1 neurons reduced lipid oxidation and accumulated excessive fat, implying the important roles of SF1 neurons in the regulation of adipose tissue function or metabolism.

DIO is associated with an accumulation of macrophages in adipose tissues. Such accumulation of macrophages in adipose tissues leads to the pro-inflammatory state which results in the secretion of adipocyte-derived inflammatory cytokines[43]. I investigated the effects of ablation and activation of SF1 neurons on inflammatory genes expression in adipose tissues. I found that ablation of SF1 neurons increased the expression of macrophage markers (F4/80, CD206, and CD11c) in ingWAT as well as associated inflammatory cytokines (Fig. 6). Enhanced MCP-1 expression mRNA levels in SF1-ablated mice imply increased macrophage recruitments into ingWAT. Furthermore, elevated TNF-α mRNA levels suggest the increased inflammatory responses in ingWAT during HFD feeding. The immunohistochemical study further strengthened these findings (Fig. 7). The crown-like structures created by macrophage aggregation surrounding adipocytes[57] were increased in the SF1-ablated mice but not in the control mice. Remarkably, the RNA-seq results confirmed my qPCR findings (Fig. 10): SF1 neuron ablation leads to an increase in inflammatory genes expression in ingWAT. Together, these results indicate that SF1 neuron ablation promotes macrophage accumulation and worsens inflammatory responses in ingWAT. In contrast, chronic activation of SF1 neurons ameliorated all above-mentioned inflammatory responses: macrophage markers and inflammatory cytokines showed a significant reduction during HFD feeding (Figs. 14 & 19).

These findings suggest that SF1 neurons in the VMH are an important regulator of inflammatory responses in the ingWAT during HFD-induced obesity.

Interestingly, the modulation of the neuronal activity of SF1 neurons in the VMH had little effect on inflammatory responses in epiWAT in DIO mice (Figs. 9 & 16). It seems that, in the regulation of inflammation, SF1 neurons have distinct effects on the different types of white adipose tissues. Different innervation patterns of the SNS among adipose tissues may account for the differences in the regulation of inflammatory responses as well as metabolic functions between ingWAT and epiWAT because ingWAT is densely innervated than epiWAT[64]. Therefore, SF1 neurons in the VMH have a protective role in inflammatory responses in ingWAT but not in epiWAT in HFD-induced obesity, as discussed below.

The present study also indicates that the modulation of SF1 neurons in the VMH reveals the effects on thermogenic genes expression as well as inflammatory responses in BAT in DIO mice (Figs. 8 & 15). Electrical stimulation of the VMH increases heat production and activates lipid metabolism in BAT[65–67]. In accordance with this, one of the important findings of this study is that when SF1 neurons were ablated, expression of thermogenic genes (UCP1, PGC-1α, and DIO2) and mitochondrial genes (CytC and CPT1b) were significantly reduced in BAT (Fig. 8). In contrast, chronic chemogenetic activation of SF1 neurons in the VMH augmented the thermogenic genes expression in BAT under HFD feeding (Fig. 15). These results suggest that SF1 neurons modulate BAT activity through these genes expression, and such reduction in BAT activity by SF1 neuron ablation contributes to the decrease in energy expenditure and body weight increase in DIO mice. However, in this study, the activation of SF1 neurons in the VMH did not significantly decrease body weight in HFD-fed mice (Figs. 12 & 17). The mechanism remains unclear. Further studies are necessary to examine the thermogenic activity of brown adipocytes in SF1-stimulated and HFD-fed mice. In addition, I need to examine the

mechanism by which chronic activation of SF1 neurons decreased the genes expression for thermogenesis in ingWAT while it increased the genes expression in BAT (Fig. 14).

The mechanisms by which SF1 neurons control adipose tissue inflammation are unclear yet. Neurons in the VMH could regulate peripheral organ function via the SNS or hormonal secretion. Previous denervation studies indicated that activation of glucose and lipid metabolism in BAT in response to the VMH stimulation is dependent on the SNS[13,67,68,69]. Direct activation of the sympathetic nerves innervating the interscapular BAT activated lipid synthesis (probably lipid turnover) in the tissue[70]. Genetic deletion of AMPK α1 subunit in the VMH SF1 neurons caused resistance to diet-induced obesity, increased BAT thermogenesis, and increased WAT browning via the SNS activation[35]. These findings suggest that VMH SF1 neurons may influence adipose tissue inflammation via the SNS. Furthermore, another study demonstrated that norepinephrine released from the SNS downregulates TNF-α expression in adipose tissues in lean mice via the β2-AR pathway[48]. Therefore, SF1 neurons may modulate adipose tissue inflammation in DIO mice through the SNS and β2-AR. Further studies with SNS denervation or adrenergic receptor knockout mice would reveal this point.

Consistent with the previous studies showing the important roles of SF1 neurons on glucose metabolism[22,27,28,31], I found that mice with SF1 neuron ablation were glucose intolerant when compared to control mice (Fig. 4). However, I have observed no differences in the ITT between control and ablated mice (Fig. 4). There could be a possibility that the impairment of glucose metabolism after ablation of SF1 neurons in the VMH is attributed in that in the liver, and relatively high dose of insulin compared to physiological levels might completely inhibit gluconeogenesis in the liver during ITT[71]. Indeed, the ablation and activation of SF1 neurons in the VMH altered liver weight reciprocally, suggesting that SF1 neurons in the VMH regulates nutrient metabolism in the liver in DIO mice. Hyperinsulinemic-euglycemic clamp study could be performed to assess the sensitivity or responsiveness of

peripheral tissues to insulin to examine the effects of VMH SF1 neurons on glucose metabolism in the liver and other peripheral tissues.

Overall, the ablation of SF1 neurons in the VMH aggravated the obesity-induced inflammatory responses in ingWAT and impaired thermogenic activity in BAT, whereas epiWAT remained unaffected. In contrast, chronic stimulation of the SF1 neurons ameliorated such inflammatory responses in ingWAT and upregulated thermogenic genes in BAT. These findings demonstrated that SF1 neurons ameliorate the impaired inflammatory responses differently in various adipose tissues and protect the function of adipose tissues in HFD-induced obesity.

References

1. Spiegelman BM, Flier JS. Obesity and the regulation of energy balance. *Cell*. 2001;104(4):531-543. doi:10.1016/S0092-8674(01)00240-9
2. Gautron L, Elmquist JK, Williams KW. Neural control of energy balance: translating circuits to therapies. *Cell*. 2015;161(1):133-145. doi: 10.1016/j.cell.2015.02.023
3. Timper K, Brüning JC. Hypothalamic circuits regulating appetite and energy homeostasis: Pathways to obesity. *DMM Disease Models and Mechanisms*. 2017;10(6):679-689. doi:10.1242/dmm.026609
4. Schneeberger M, Gomis R, Claret M. Hypothalamic and brainstem neuronal circuits controlling homeostatic energy balance. *Journal of Endocrinology*. 2014;220(2):25-46. doi:10.1530/JOE-13-0398
5. Brooks CM, Lockwood RA, Wiggins ML. A study of the effect of hypothalamic lesions on the eating habits of the albino rat. *The American Journal of Physiology*. 1946;147(4):735-741. doi:10.1152/ajplegacy.1946.147.4.735
6. Balagura S, Devenport LD. Feeding patterns of normal and ventromedial hypothalamic lesioned male and female rats. *Journal of Comparative and Physiological Psychology*. 1970;71(3):357-364. doi:10.1037/h0029118
7. Becker EE, Kissileff HR. Inhibitory controls of feeding by the ventromedial hypothalamus. *American Journal of Physiology*. 1974;226(2):383-396. doi:10.1152-/ajplegacy.1974.226.2.383
8. Satoh N, Ogawa Y, Katsuura G, et al. Pathophysiological significance of the obese gene product, leptin, in ventromedial hypothalamus (VMH) lesioned rats: evidence for loss of its satiety effect in VMH-lesioned rats. *Endocrinology*. 1997;138(3):947-954. doi:10.1210/endo.138.3.4989

9. Shimazu T, Fukuda A, Ban T. Reciprocal influences of the ventromedial and lateral hypothalamic nuclei on blood glucose level and liver glycogen content. *Nature*. 1966;210(5041):1178-1179. doi:10.1038/2101178a0
10. Shimazu T, Matsushita H, Ishikawa K. Hypothalamic control of liver glycogen metabolism in adult and aged rats. *Brain Research*. 1978;144(2):343-352. doi:10.1016/0006-8993(78)90159-2
11. Takahashi A, Shimazu T. Hypothalamic regulation of lipid metabolism in the rat: effect of hypothalamic stimulation on lipolysis. *Journal of the Autonomic Nervous System*. 1981;4(3):195-206. doi:10.1016/0165-1838(81)90044-8
12. Sudo M, Minokoshi Y, Shimazu T. Ventromedial hypothalamic stimulation enhances peripheral glucose uptake in anesthetized rats. *American Journal of Physiology - Endocrinology and Metabolism*. 1991;261(3): E298-E303. doi:10.1152/ajpendo.1991.261.3. e298
13. Ruffin MP, Nicolaidis S. Electrical stimulation of the ventromedial hypothalamus enhances both fat utilization and metabolic rate that precede and parallel the inhibition of feeding behavior. *Brain Research*. 1999;846(1):23-29. doi:10.1016/S00068993-(99)01922-8
14. Minokoshi Y, Haque MS, Shimazu T. Microinjection of leptin into the ventromedial hypothalamus increases glucose uptake in peripheral tissues in rats. *Diabetes*. 1999;48(2):287-291. doi:10.2337/diabetes.48.2.287
15. Toda C, Shiuchi T, Lee S, et al. Distinct effects of leptin and a melanocortin receptor agonist injected into medial hypothalamic nuclei on glucose uptake in peripheral tissues. *Diabetes*. 2009;58(12):2757-2765. doi:10.2337/db09-0638

16. Minokoshi Y, Kim YB, Peroni OD, et al. Leptin stimulates fatty-acid oxidation by activating AMP-activated protein kinase. *Nature*. 2002;415(6869):339-343. doi:10.1038/415339a
17. Shiuchi T, Haque MS, Okamoto S, et al. Hypothalamic orexin stimulates feeding-associated glucose utilization in skeletal muscle via sympathetic nervous system. *Cell Metabolism*. 2009;10(6):466-480. doi: 10.1016/j.cmet.2009.09.013
18. Gaur A, Pal GK, Ananthanarayanan PH, Pal P. Role of ventromedial hypothalamus in high fat diet induced obesity in male rats: Association with lipid profile, thyroid profile and insulin resistance. *Annals of Neurosciences*. 2014;21(3):104-107. doi:10.5214/ans.0972.7531.210306
19. Segal JP, Stallings NR, Lee CE, et al. Use of laser-capture microdissection for the identification of marker genes for the ventromedial hypothalamic nucleus. *Journal of Neuroscience*. 2005;25(16):4181-4188. doi:10.1523/JNEUROSCI.0158-05.2005
20. Kurrasch DM, Cheung CC, Lee FY, Tran P v., Hata K, Ingraham HA. The neonatal ventromedial hypothalamus transcriptome reveals novel markers with spatially distinct patterning. *Journal of Neuroscience*. 2007;27(50):13624-13634. doi:10.1523/JNEUROSCI.2858-07.2007
21. Kim DW, Yao Z, Graybuck LT, et al. Multimodal analysis of cell types in a hypothalamic node controlling social behavior. *Cell*. 2019;179(3):713-728.e17. doi: 10.1016/j.cell.2019.09.020
22. Choi YH, Fujikawa T, Lee J, Reuter A, Kim KW. Revisiting the ventral medial nucleus of the hypothalamus: The roles of SF-1 neurons in energy homeostasis. *Frontiers in Neuroscience*. 2013;7(71). doi:10.3389/fnins.2013.00071

23. Morohashi K, Hatano O, Nomura M, et al. Function and distribution of a steroidogenic cell-specific transcription factor, Ad4BP. *Journal of Steroid Biochemistry and Molecular Biology*. 1995;53(1-6):81-88. doi:10.1016/0960-0760(95)00041

24. Ikeda Y, Luo X, Abbud R, Nilson JH, Parker KL. The nuclear receptor steroidogenic factor 1 is essential for the formation of the ventromedial hypothalamic nucleus. *Molecular Endocrinology*. 1995;9(4):478-486. doi:10.1210/mend.9.4.7659091

25. Shinoda K, Lei H, Yoshii H, et al. Developmental defects of the ventromedial hypothalamic nucleus and pituitary gonadotroph in the Ftz-F1 disrupted mice. *Developmental Dynamics*. 1995;204(1):22-29. doi:10.1002/aja.1002040104

26. Tran P v., Lee MB, Marín O, et al. Requirement of the orphan nuclear receptor SF-1 in terminal differentiation of ventromedial hypothalamic neurons. *Molecular and Cellular Neuroscience*. 2003;22(4):441-453. doi:10.1016/S1044-7431(03)00027-7

27. Meek TH, Nelson JT, Matsen ME, et al. Functional identification of a neurocircuit regulating blood glucose. *Proceedings of the National Academy of Sciences*. 2016;113(14): E2073-E2082. doi:10.1073/pnas.1521160113

28. Coutinho EA, Okamoto S, Ishikawa AW, et al. Activation of SF1 neurons in the ventromedial hypothalamus by DREADD technology increases insulin sensitivity in peripheral tissues. *Diabetes*. 2017;66(9):2372-2386. doi:10.2337/db16-1344

29. Dhillon H, Zigman JM, Ye C, et al. Leptin directly activates SF1 neurons in the VMH, and this action by leptin is required for normal body-weight homeostasis. *Neuron*. 2006;49(2):191-203. doi: 10.1016/j.neuron.2005.12.021

30. Bingham NC, Anderson KK, Reuter AL, Stallings NR, Parker KL. Selective loss of leptin receptors in the ventromedial hypothalamic nucleus results in increased adiposity and a metabolic syndrome. *Endocrinology*. 2008;149(5):2138-2148. doi:10.1210/en.2007-1200

31. Tong Q, Ye CP, McCrimmon RJ, et al. Synaptic glutamate release by ventromedial hypothalamic neurons is part of the neurocircuitry that prevents hypoglycemia. *Cell Metabolism*. 2007;5(5):383-393. doi: 10.1016/j.cmet.2007.04.001

32. Klöckener T, Hess S, Belgardt BF, et al. High-fat feeding promotes obesity via insulin receptor/PI3K-dependent inhibition of SF-1 VMH neurons. *Nature Neuroscience*. 2011;14(7):911-918. doi:10.1038/nn.2847

33. Chiappini F, Catalano KJ, Lee J, et al. Ventromedial hypothalamus-specific Ptpn1 deletion exacerbates diet-induced obesity in female mice. *Journal of Clinical Investigation*. 2014;124(9):3781-3792. doi:10.1172/JCI68585

34. Sohn JW, Oh Y, Kim KW, Lee S, Williams KW, Elmquist JK. Leptin and insulin engage specific PI3K subunits in hypothalamic SF1 neurons. *Molecular Metabolism*. 2016;5(8):669-679. doi: 10.1016/j.molmet.2016.06.004

35. Seoane-Collazo P, Roa J, Rial-Pensado E, et al. SF1-specific AMPKa1 deletion protects against diet-induced obesity. *Diabetes*. 2018;67(11):2213-2226. doi:10.2337/db17-1538

36. Kershaw EE, Flier JS. Adipose tissue as an endocrine organ. *The Journal of Clinical Endocrinology and Metabolism*. 2004;89(6):2548-2556. doi:10.1210/jc.2004-0395

37. Weisberg SP, McCann D, Desai M, Rosenbaum M, Leibel RL, Ferrante AW. Obesity is associated with macrophage accumulation in adipose tissue. *Journal of Clinical Investigation*. 2003;112(12):1796-1808. doi:10.1172/jci19246

38. Xu H, Barnes GT, Yang Q, et al. Chronic inflammation in fat plays a crucial role in the development of obesity-related insulin resistance. *Journal of Clinical Investigation*. 2003;112(12):1821-1830. doi:10.1172/jci19451

39. Lumeng CN, Bodzin JL, Saltiel AR. Obesity induces a phenotypic switch in adipose tissue macrophage polarization. *Journal of Clinical Investigation*. 2007;117(1):175-184. doi:10.1172/JCI29881

40. Chait A, den Hartigh LJ. Adipose tissue distribution, inflammation and its metabolic consequences, including diabetes and cardiovascular disease. *Frontiers in Cardiovascular Medicine*. 2020;7:22. doi:10.3389/fcvm.2020.00022

41. Ellulu MS, Patimah I, Khaza'ai H, Rahmat A, Abed Y. Obesity & inflammation: The linking mechanism & the complications. *Archives of Medical Science*. 2017;13(4):851-863. doi:10.5114/aoms.2016.58928

42. Russo L, Lumeng CN. Properties and functions of adipose tissue macrophages in obesity. *Immunology*. 2018;155(4):407-417. doi:10.1111/imm.13002

43. Coppack SW. Pro-inflammatory cytokines and adipose tissue. *Proceedings of the Nutrition Society*. 2001;60(3):349-356. doi:10.1079/pns2001110

44. Makki K, Froguel P, Wolowczuk I. Adipose tissue in obesity-related inflammation and insulin resistance: cells, cytokines, and chemokines. *International Scholarly Research Notices*. 2013;2013:12. doi:10.1155/2013/139239

45. Zatterale F, Longo M, Naderi J, et al. Chronic adipose tissue inflammation linking obesity to insulin resistance and type 2 diabetes. *Frontiers in Physiology*. 2020;10:1607. doi:10.3389/fphys.2019.01607

46. Ben-Shaanan TL, Azulay-Debby H, Dubovik T, et al. Activation of the reward system boosts innate and adaptive immunity. *Nature Medicine*. 2016;22(8):940-944. doi:10.1038/nm.4133

47. Zhang X, Lei B, Yuan Y, et al. Brain control of humoral immune responses amenable to behavioural modulation. *Nature*. 2020;581(7807):204-208. doi:10.1038/s41586-020-2235-7

48. Tang L, Okamoto S, Shiuchi T, et al. Sympathetic nerve activity maintains an anti-inflammatory state in adipose tissue in male mice by inhibiting TNF-α gene expression in macrophages. *Endocrinology*. 2015;156(10):3680-3694. doi:10.1210/EN.2015-1096

49. Paxinos G, Franklin K. The mouse brain in stereotaxic coordinates. 3rd Edition. San Diego, California: Academic Press 2007. https://www.elsevier.com/books/the-mouse-brain-in-stereotaxic-coordinates-compact/franklin/978-0-12-374244-5

50. Ishihara K, Oyaizu S, Onuki K, Lim K, Fushiki T. Chronic (-)-hydroxycitrate administration spares carbohydrate utilization and promotes lipid oxidation during exercise in mice. *Journal of Nutrition*. 2000;130(12):2990-2995. doi:10.1093/jn/130.12.2990

51. Chi J, Crane A, Wu Z, Cohen P. Adipo-clear: A tissue clearing method for three-dimensional imaging of adipose tissue. *Journal of Visualized Experiments*. 2018;2018(137):58271. doi:10.3791/58271

52. Chen S, Zhou Y, Chen Y, Gu J. Fastp: An ultra-fast all-in-one FASTQ preprocessor. In: *Bioinformatics*. 2018;34(17):i884-i890. doi:10.1093/bioinformatics/bty560

53. Bray NL, Pimentel H, Melsted P, Pachter L. Near-optimal probabilistic RNA-seq quantification. *Nature Biotechnology*. 2016;34(5):525-527. doi:10.1038/nbt.3519

54. Soneson C, Love MI, Robinson MD. Differential analyses for RNA-seq: Transcript-level estimates improve gene-level inferences. *F1000Research*. 2016;4. doi:10.12688/F1000RESEARCH.7563.2

55. Love MI, Huber W, Anders S. Moderated estimation of fold change and dispersion for RNA-seq data with DESeq2. *Genome Biology*. 2014;15(12):550. doi:10.1186/s13059-014-0550-

56. Luo W, Friedman MS, Shedden K, Hankenson KD, Woolf PJ. GAGE: Generally applicable gene set enrichment for pathway analysis. *BMC Bioinformatics*. 2009;10(1):1-17. doi:10.1186/1471-2105-10-161

57. Murano I, Barbatelli G, Parisani V, et al. Dead adipocytes, detected as crown-like structures, are prevalent in visceral fat depots of genetically obese mice. *Journal of Lipid Research*. 2008;49(7):1562-1568. doi:10.1194/jlr.M800019-JLR200

58. Seale P, Lazar MA. Brown fat in humans: Turning up the heat on obesity. *Diabetes*. 2009;58(7):1482-1484. doi:10.2337/db09-0622

59. Morrison SF, Madden CJ, Tupone D. Central neural regulation of brown adipose tissue thermogenesis and energy expenditure. *Cell Metabolism*. 2014;19(5):741-756. doi: 10.1016/j.cmet.2014.02.007

60. Caprio M, Infante M, Guglielmi V, et al. Brown adipose tissue, diet-induced thermogenesis, and thermogenic food ingredients: from mice to men. *Frontiers in Endocrinology*. 2020; 11:222. doi:10.3389/fendo.2020.00222

61. Seale P, Conroe HM, Estall J, et al. Prdm16 determines the thermogenic program of subcutaneous white adipose tissue in mice. *Journal of Clinical Investigation*. 2011;121(1):96-105. doi:10.1172/JCI44271

62. Kajimura S, Spiegelman BM, Seale P. Brown and beige fat: physiological roles beyond heat generation. *Cell Metabolism*. 2015;22(4):546-559. doi: 10.1016/j.cmet. 2015.09.007

63. Ikeda K, Yamada T. UCP1 dependent and independent thermogenesis in brown and beige adipocytes. *Frontiers in Endocrinology*. 2020;11:498. doi:10.3389/fendo. 2020.00498

64. Chi J, Wu Z, Choi CHJ, et al. Three-dimensional adipose tissue imaging reveals regional variation in beige fat biogenesis and PRDM16-dependent sympathetic neurite Density. *Cell Metabolism*. 2018;27(1):226-236.e3. doi: 10.1016/j.cmet.2017.12.011
65. Shimazu T, Takahashi A. Stimulation of hypothalamic nuclei has differential effects on lipid synthesis in brown and white adipose tissue. *Nature*. 1980;284(5751):62-63. doi:10.1038/284062a0
66. Perkins MN, Rothwell NJ, Stock MJ, Stone TW. Activation of brown adipose tissue thermogenesis by the ventromedial hypothalamus. *Nature*. 1981;289(5796):401-402. doi:10.1038/289401a0
67. Minokoshi Y, Saito M, Shimazu T. Sympathetic denervation impairs responses of brown adipose tissue to VMH stimulation. *American Journal of Physiology-Regulatory Integrative and Comparative Physiology*. 1986;251(5): R1005-R1008. doi:10.1152/ajpregu.1986.251.5. r1005
68. Saito M, Minokoshi Y, Shimazu T. Ventromedial hypothalamic stimulation accelerates norepinephrine turnover in brown adipose tissue of rats. *Life Sciences*. 1987;41(2):193-197. doi:10.1016/0024-3205(87)90493-0
69. Shimazu T, Sudo M, Minokoshi Y, Takahashi A. Role of the hypothalamus in insulin-independent glucose uptake in peripheral tissues. *Brain Research Bulletin*. 1991;27(3-4):501-504. doi:10.1016/0361-9230(91)90149-E
70. Minokoshi Y, Saito M, Shimazu T. Sympathetic activation of lipid synthesis in brown adipose tissue in the rat. *The Journal of Physiology*. 1988;398(1):361-370. doi:10.1113/jphysiol. 1988.sp017047
71. Edgerton DS, Cardin S, Emshwiller M, et al. Small Increases in Insulin Inhibit Hepatic Glucose Production Solely Caused by an Effect on Glycogen Metabolism. *Diabetes*. 2001;50(8):1872-1882. doi:10.2337/diabetes.50.8.1872

Figure 1

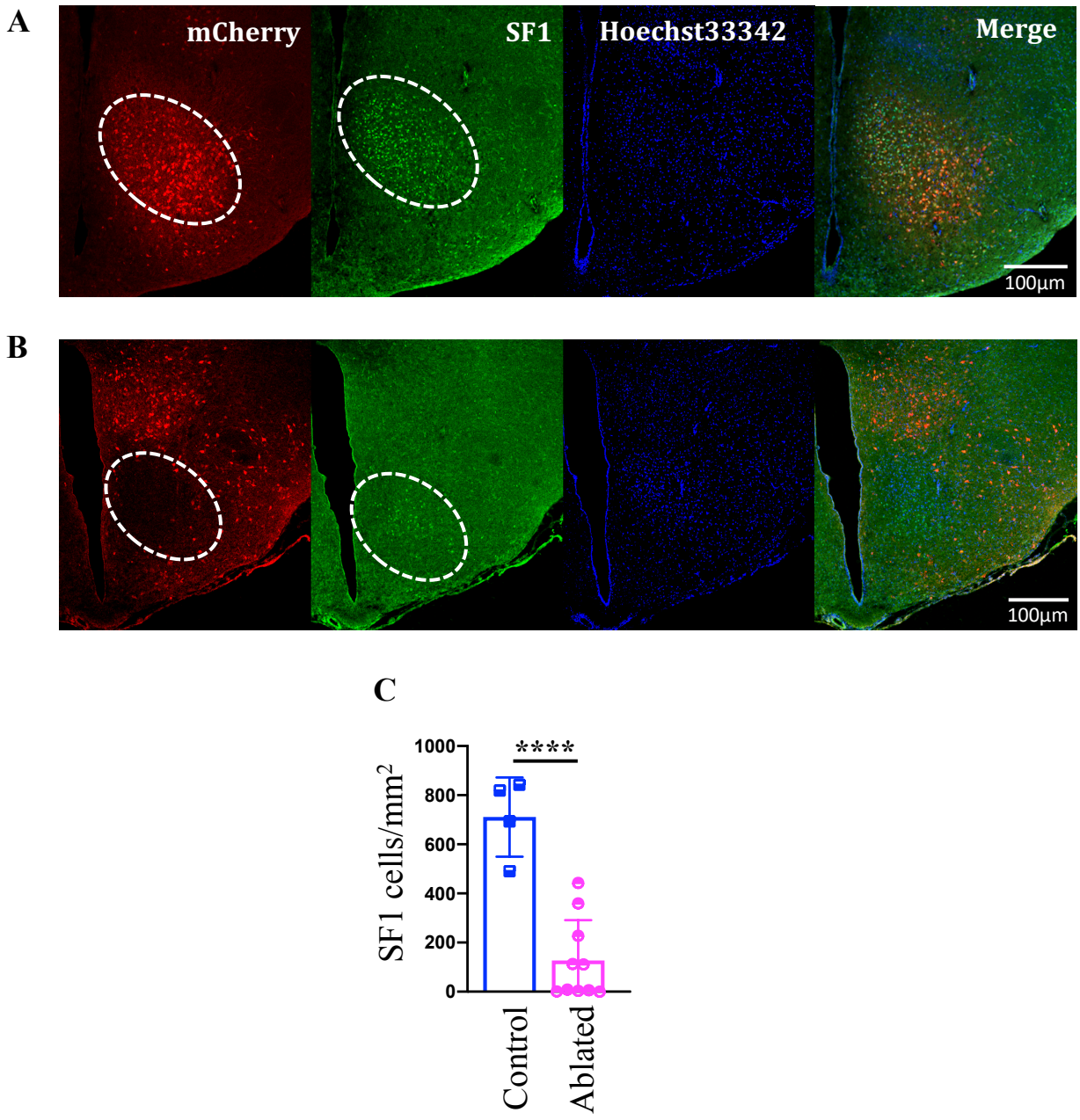

Figure 1: Specific expression of diphtheria toxin-A ablated SF1 neurons in the VMH

(A, B) Adeno-associated viruses (AAVs) that express mCherry in the absence of Cre recombinase but express diphtheria toxin-A (DTA) subunit in the presence of Cre (AAV-FLEX-DTA) were injected into the vicinity of the VMH area. Virus-injected brain sections containing the VMH from wildtype (A) or SF1-Cre mice (B) were immunostained for mCherry (red) and SF1 (green). Sections were counterstained with Hoechst33342 (blue) for nuclear

staining. Merged images are shown on the right (Merge). (C) A histogram shows the number of SF1 positive cells per square millimeter of VMH in wildtype (n=4) and SF1-Cre mice (n=10) injected with AAV-FLEX-DTA. Dotted circles representing the VMH area in the section. All data are shown in mean ± SD. ****p< 0.0001, unpaired *t*-test. Scatter plot displays the data for individual mice. Ablated, SF1-ablated mice; Control, WT control mice.

Figure 2

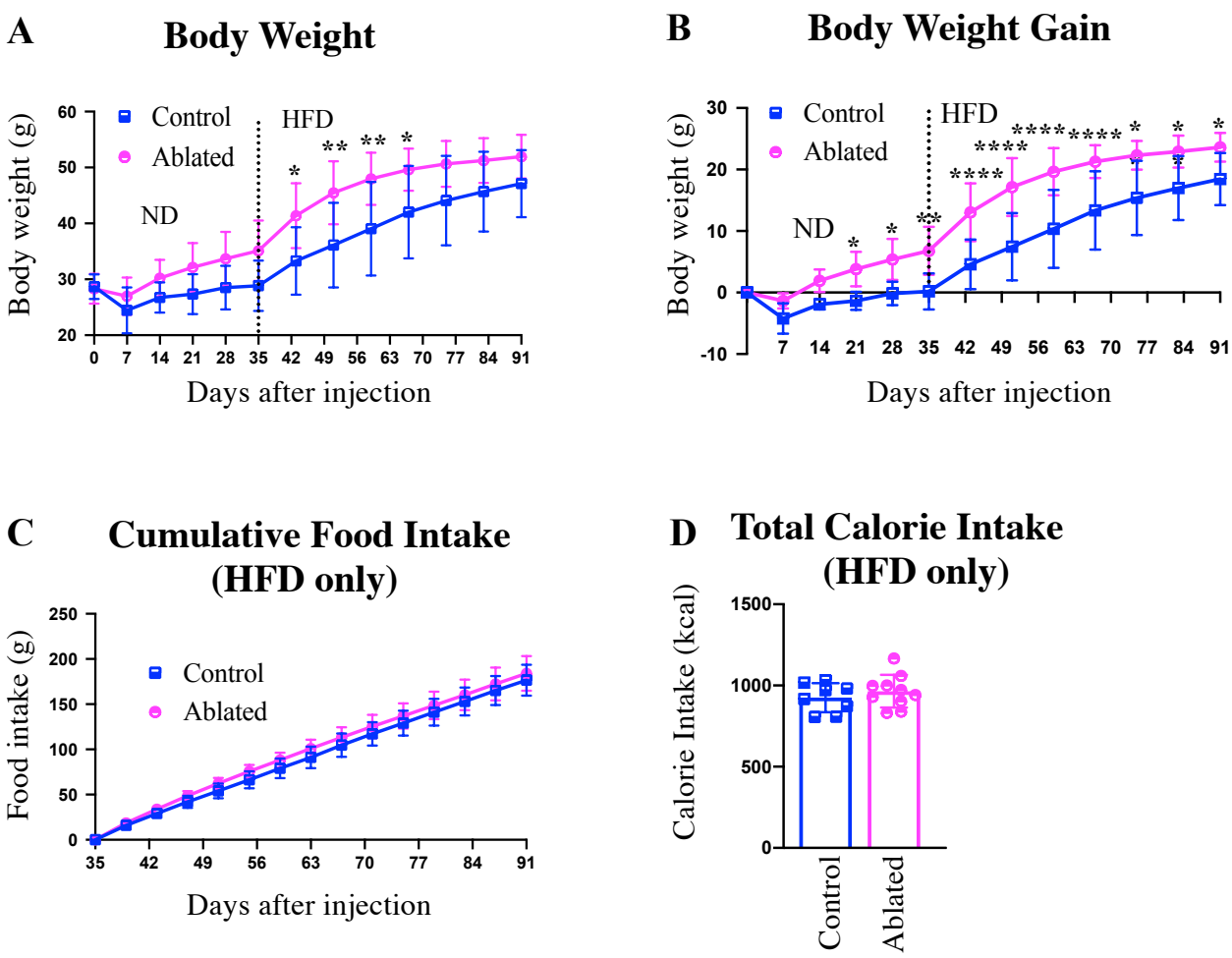

Figure 2: Effects of SF1 neuron ablation on HFD-induced increase in body weight and food intake.

(A, B) Body weight (A) and body weight gain (B) in control and SF1-ablated mice. Day 0 is the day when AAVs were injected. After 5 weeks (35 days) with normal diet feeding (ND), mice were fed with a high-fat diet (HFD). (C) Cumulative food intake during HFD feeding period. (D) Total calorie intake during HFD feeding period. n=8 for control mice and n=10 for SF1-ablated mice. All data are shown in mean ± SD. *P < 0.05, **P < 0.01, ****P < 0.0001, two-way ANOVA test with post-hoc Sidak's test (A, B, C) and unpaired t-test (D). Scatter plot displays the data for individual mice. Ablated, SF1-ablated mice; Control, WT control mice.

Figure 3

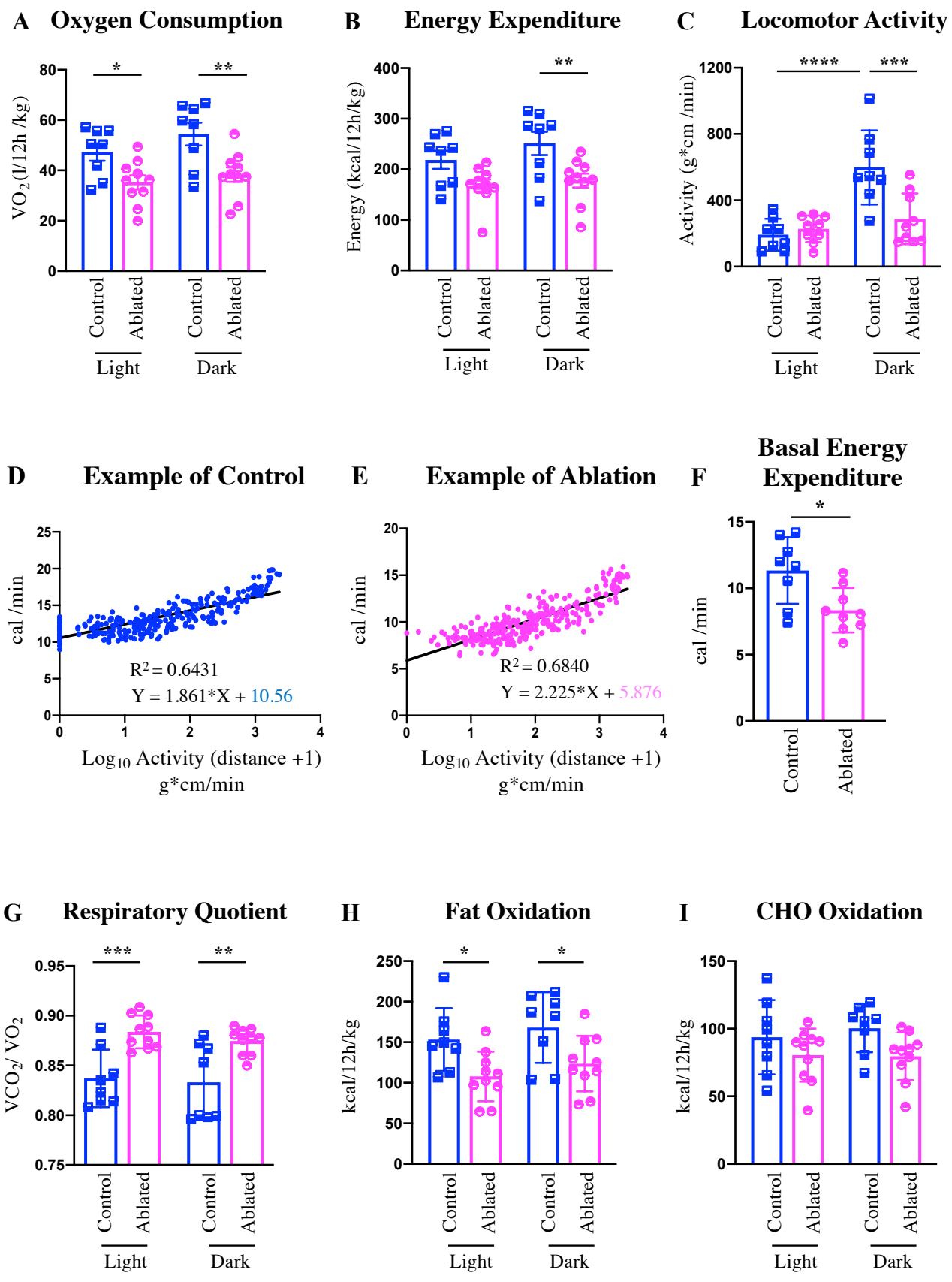
A Oxygen Consumption
B Energy Expenditure
C Locomotor Activity
VO2 (l/12h /kg)
Energy (kcal/12h/kg)
Activity (g*cm /min)
Control
Ablated
Light
Dark
D Example of Control
E Example of Ablation
F Basal Energy Expenditure
cal /min
R2 = 0.6431
Y = 1.861*X + 10.56
R2 = 0.6840
Y = 2.225*X + 5.876
Log10 Activity (distance +1)
g*cm/min
G Respiratory Quotient
H Fat Oxidation
I CHO Oxidation
VCO2/ VO2
kcal/12h/kg

Figure 3: Effects of SF1 neuron ablation on energy expenditure and respiratory quotient of DIO mice.

(A - C) Total oxygen consumption per kg body weight (A), total energy expenditure per kg body weight (B), and locomotor activity (C) during light and dark periods of SF1-ablated and control mice. (D, E) A representative example from control (D) or SF1-ablated mice (E) of a linear regression between locomotor activity and energy expenditure to calculate basal energy expenditure. Y-intersects show the basal energy expenditure of the respective mouse. (F) Calculated basal energy expenditure of control and SF1-ablated mice. (G - I) Respiratory quotient (RQ) (G), fat oxidation (H), and carbohydrate (CHO) oxidation (I) during light and dark periods in SF1-ablated and control mice. Mice were fed with HFD for 8 weeks as shown in the text and Figure 2. n=8 for control mice and n=10 for SF1-ablated mice. n=9 for SF1-ablated mice (C, F). All data are shown in mean ± SD. *$P < 0.05$, **$P < 0.01$, ***$P < 0.001$, ****$P < 0.0001$, two-way ANOVA with post-hoc Sidak's test (A-C, G-H) and unpaired *t*-test (D). Scatter plots display the data for individual mice. Ablated, SF1-ablated mice; Control, WT control mice.

Figure 4

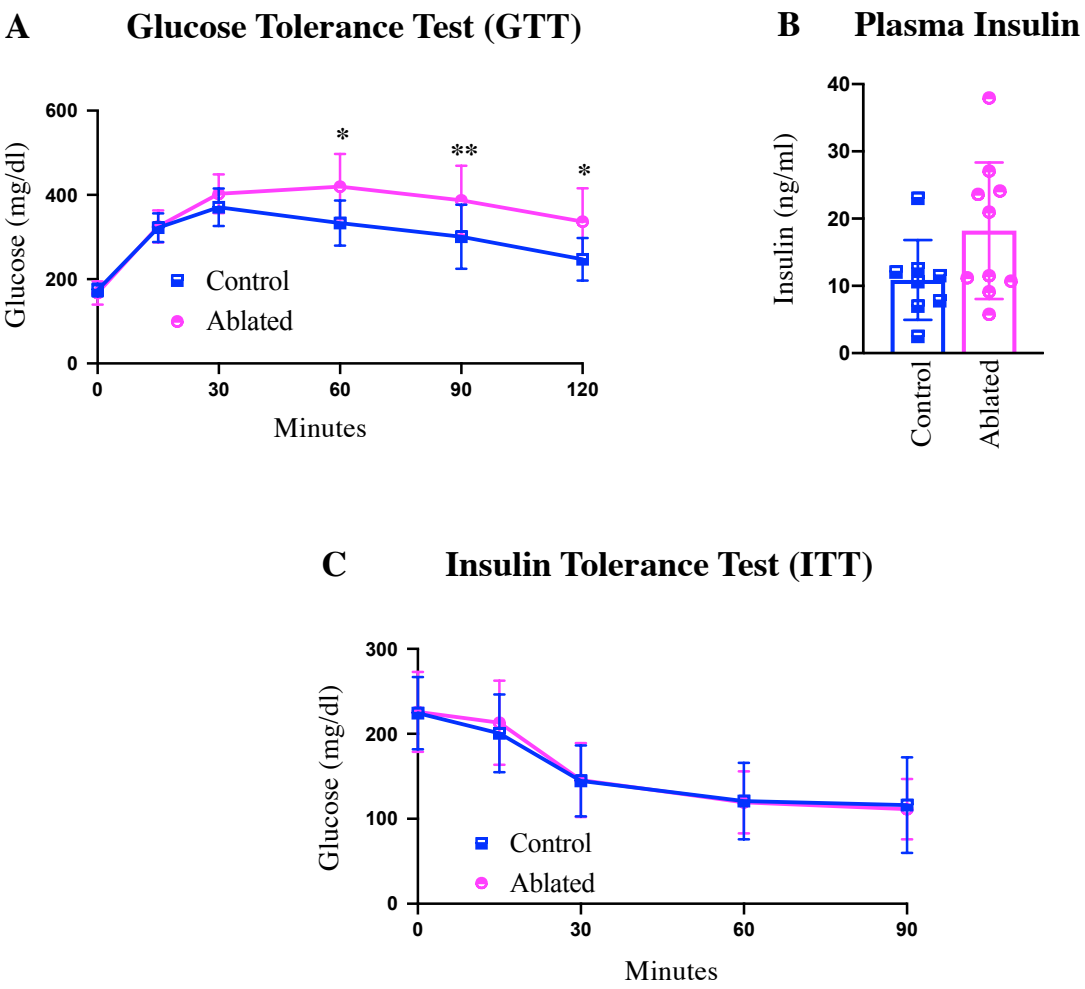

Figure 4: Effects of SF1 neuron ablation on glucose metabolism of DIO mice.

(A) Blood glucose levels after intraperitoneal injection of glucose (1 g/kg BW) in control and SF1-ablated mice. (B) Plasma insulin levels after 3 hours of fasting. (C) Blood glucose levels after intraperitoneal injection of insulin (0.5 U/kg BW). Mice were fed with HFD for 8 weeks as shown in the text and Figure 2. n=8 for control and n=10 for SF1-ablated mice. All data are shown in mean ± SD. *P < 0.05, **P < 0.01, two-way ANOVA with post-hoc Sidak's test (A, C) and unpaired *t*-test (B). Scatter plots display the data for individual mice. Ablated, SF1-ablated mice; Control, WT control mice

Figure 5

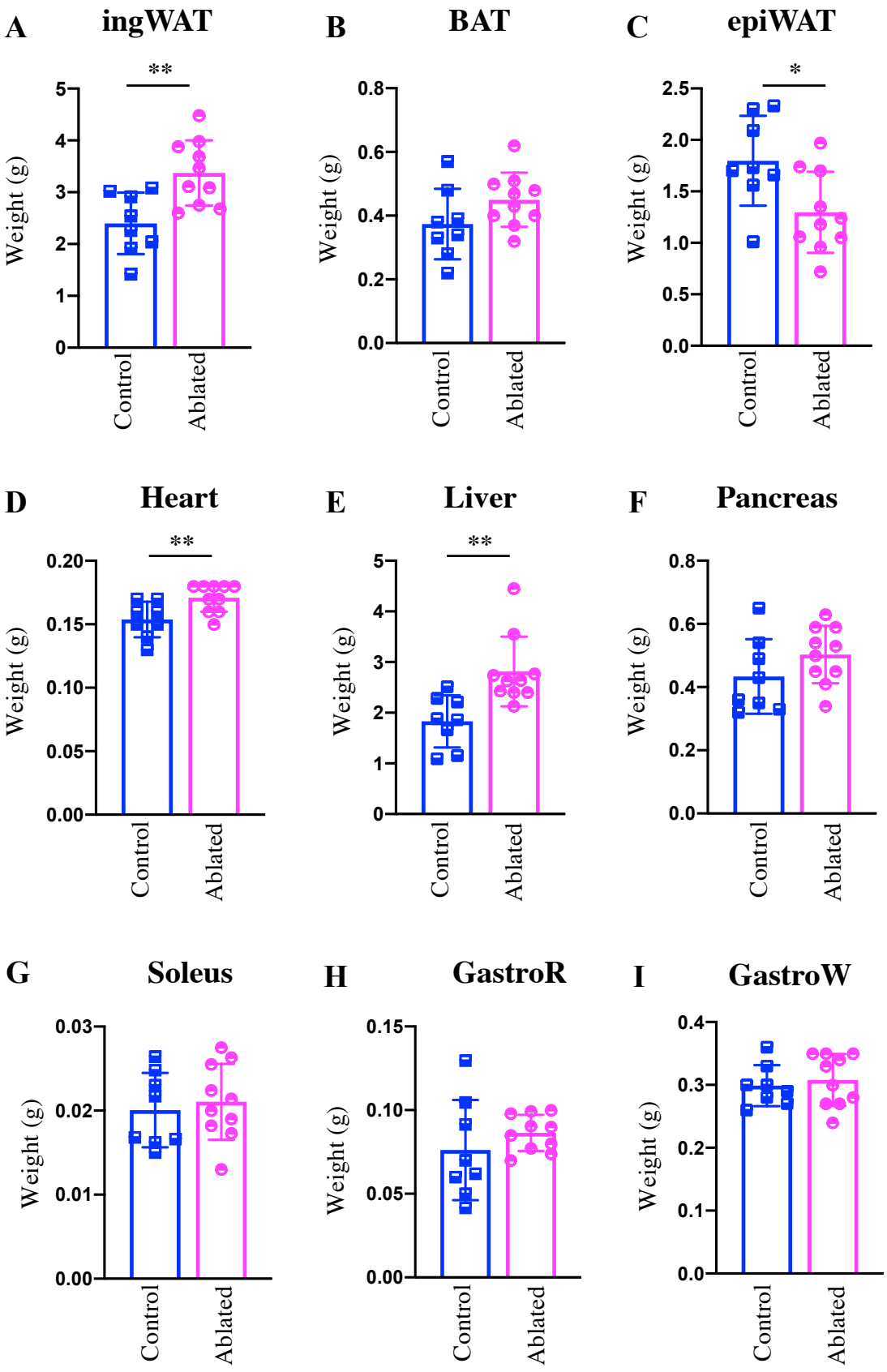
A
ingWAT
**
Weight (g)
5
4
3
2
1
0
Control
Ablated
B
BAT
Weight (g)
0.8
0.6
0.4
0.2
0.0
Control
Ablated
C
epiWAT
*
Weight (g)
2.5
2.0
1.5
1.0
0.5
0.0
Control
Ablated
D
Heart
**
Weight (g)
0.20
0.15
0.10
0.05
0.00
Control
Ablated
E
Liver
**
Weight (g)
5
4
3
2
1
0
Control
Ablated
F
Pancreas
Weight (g)
0.8
0.6
0.4
0.2
0.0
Control
Ablated
G
Soleus
Weight (g)
0.03
0.02
0.01
0.00
Control
Ablated
H
GastroR
Weight (g)
0.15
0.10
0.05
0.00
Control
Ablated
I
GastroW
Weight (g)
0.4
0.3
0.2
0.1
0.0
Control
Ablated

Figure 5: Effects of SF1 neuron ablation on the weight of peripheral tissues of DIO mice. Tissue weights of inguinal WAT (ingWAT) (A), brown adipose tissue (BAT) (B), epididymal WAT (epiWAT) (C), heart (D), liver (E), pancreas (F), and three regions of skeletal muscles [soleus (G), red part of gastrocnemius (GastroR) (H), and white part of gastrocnemius (GastroW) (I)] of control and SF1-ablated mice. Mice were fed with HFD for 8 weeks as shown in the text and Figure 2. n=8 for control mice and n=10 for SF1-ablated mice. All data are shown in ± SD. *$P < 0.05$, **$P < 0.01$, unpaired *t*-test. Scatter plots display the data for individual mice. Ablated, SF1-ablated mice; Control, WT control mice.

Figure 6

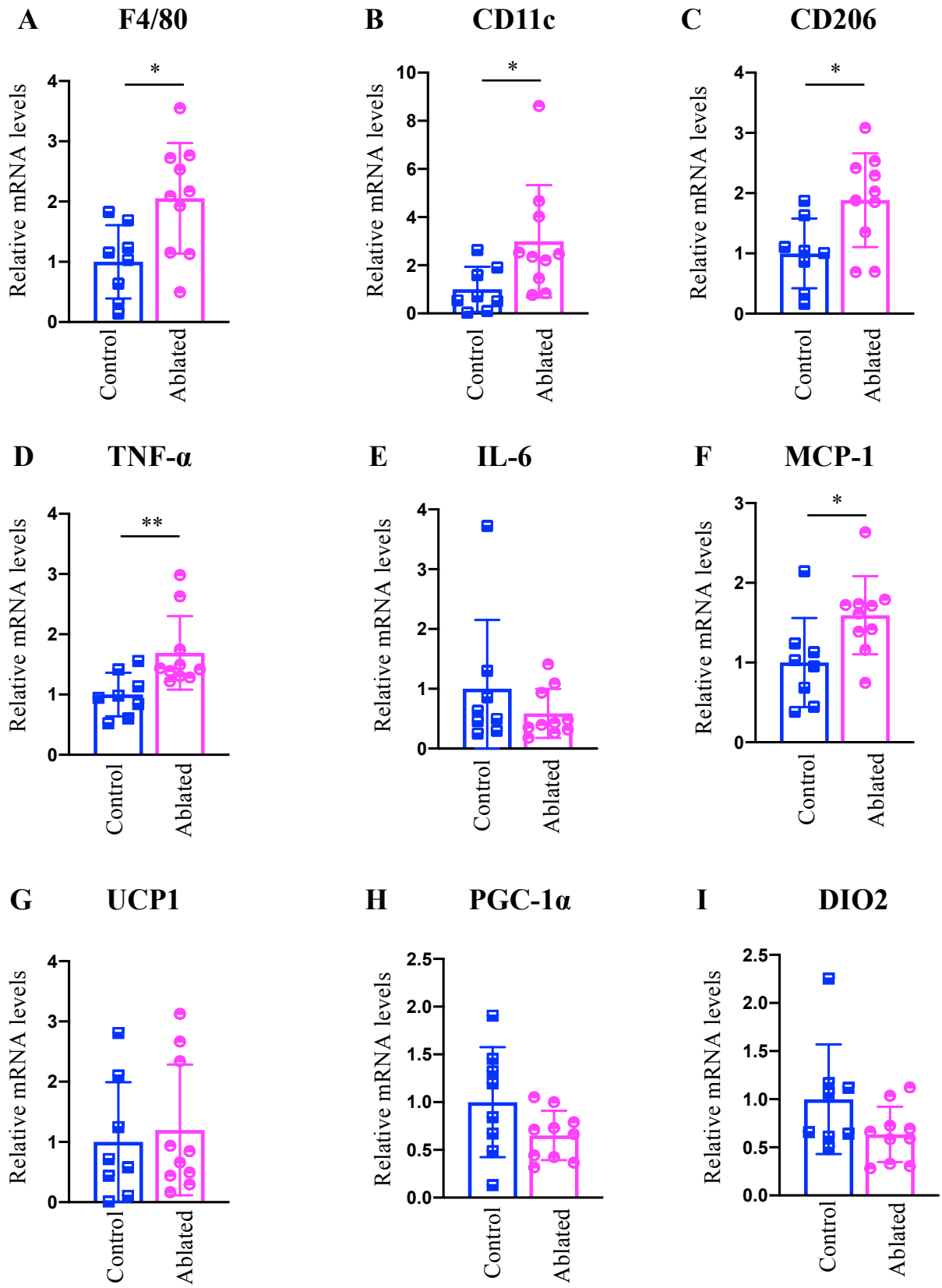
A
F4/80
B
CD11c
C
CD206
D
TNF-α
E
IL-6
F
MCP-1
G
UCP1
H
PGC-1α
I
DIO2
Relative mRNA levels
Control
Ablated
*
**

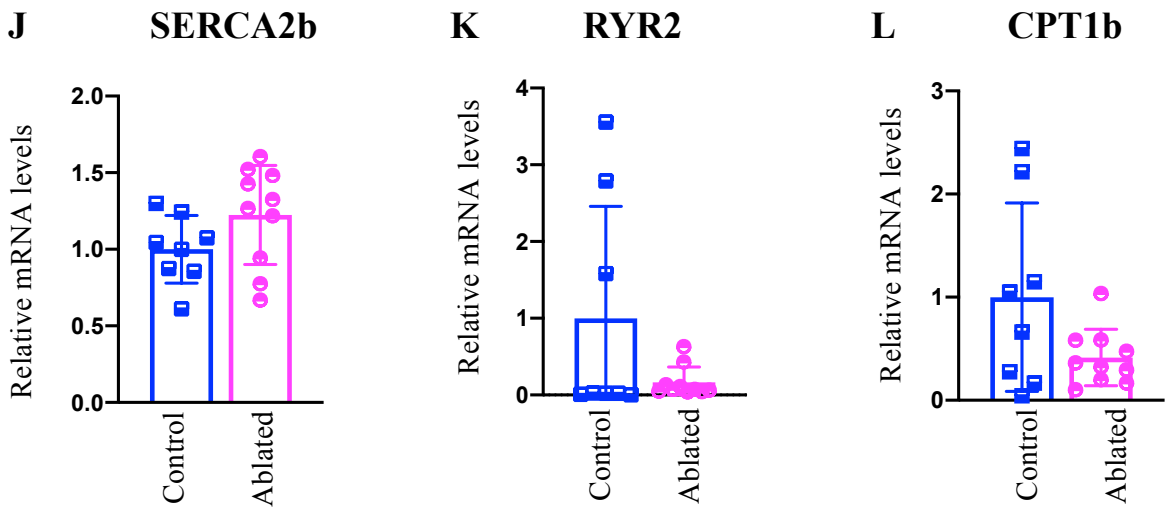

Figure 6: Effects of SF1 neuron ablation on genes expression in ingWAT of DIO mice.

Relative mRNA abundances of macrophage markers [F4/80 (A), CD11c (B), and CD206 (C)], inflammatory cytokines [TNF-α (D), IL-6 (E), and MCP-1 (F)], thermogenesis-related genes [uncoupling protein 1 (UCP1) (G), peroxisome proliferator-activated receptor gamma coactivator-1 alpha (PGC-1α) (H), and iodothyronine deiodinase 2 (DIO2) (I)], and mitochondrial genes [sarcoplasmic/endoplasmic reticulum calcium ATPase 2b (SERCA2b) (J), ryanodine receptor 2 (RYR2) (K), and carnitine palmitoyltransferase 1b (CPT1b) (L)] in ingWAT of control and SF1-ablated mice. Mice were fed with HFD for 8 weeks as shown in the text and Figure 2. n=8 for control mice and n=10 for SF1-ablated mice. All data are shown in ± SD. *P < 0.05, **P < 0.01, unpaired *t*-test. Scatter plots display the data for individual mice. Ablated, SF1-ablated mice; Control, WT control mice.

Figure 7

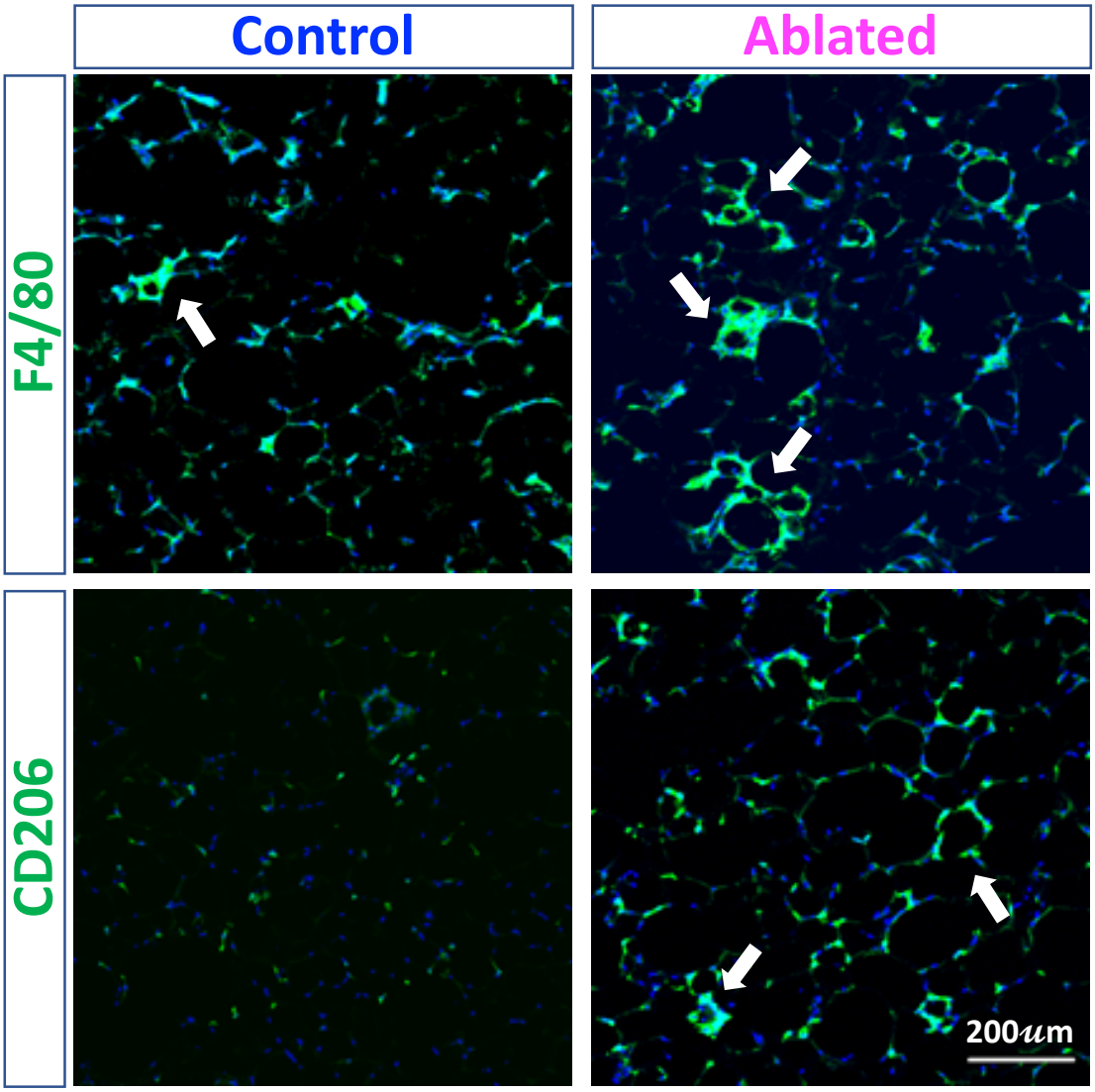

Figure 7: Increased number of macrophage marker positive cells in ingWAT of DIO mice after ablation of SF1 neurons.

Representative ingWAT images showing immunoreactivity for macrophage markers (F4/80 and CD206, green) in control and SF1-ablated mice (A). Sections were counterstained with Hoechst33342 for nuclear staining (blue). White arrows indicate crown-like structures. Mice were fed with HFD for 8 weeks as shown in the text and Figure 2.

Figure 8

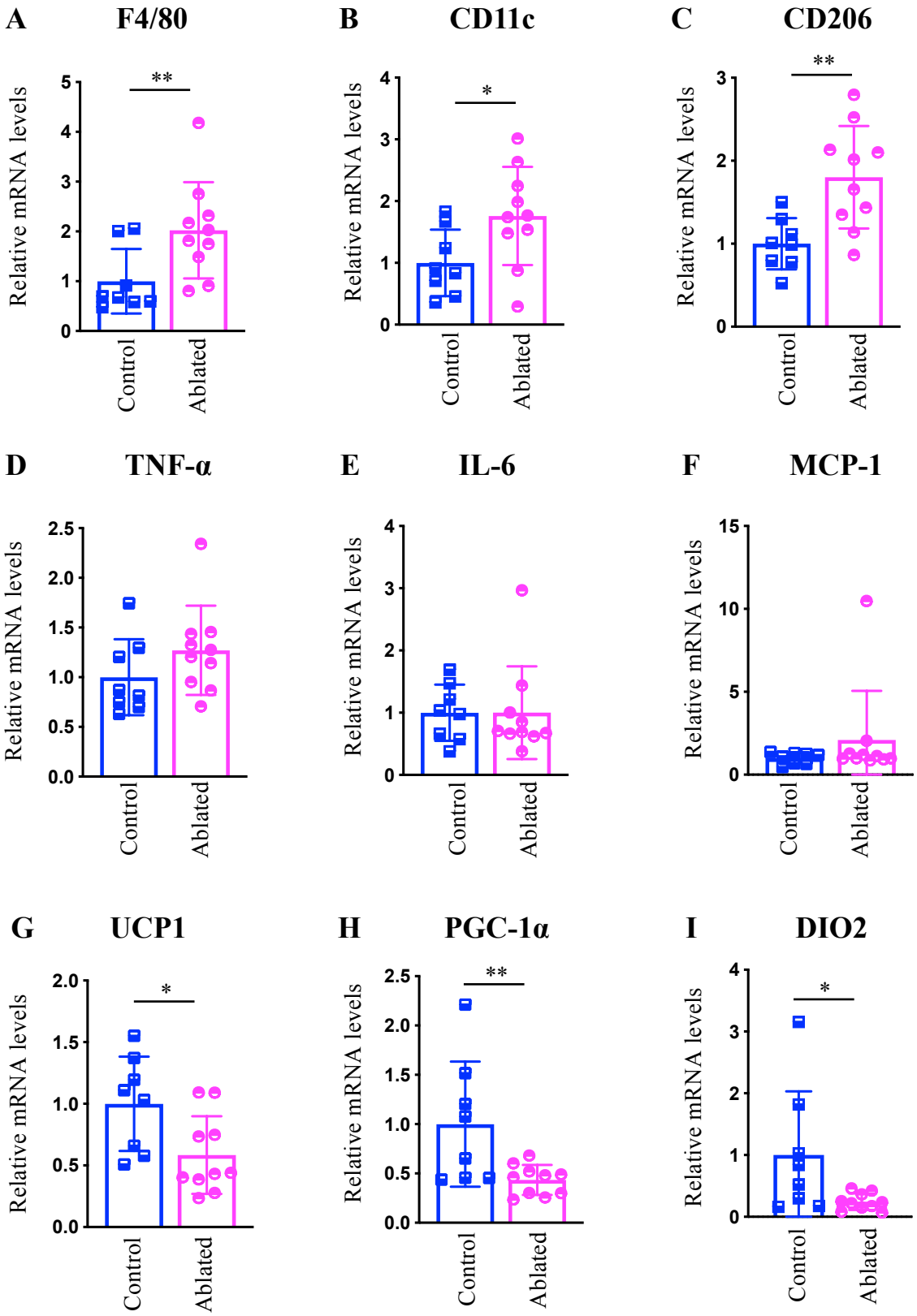
A
F4/80
B
CD11c
C
CD206
D
TNF-α
E
IL-6
F
MCP-1
G
UCP1
H
PGC-1α
I
DIO2
Relative mRNA levels
Control
Ablated
**
*

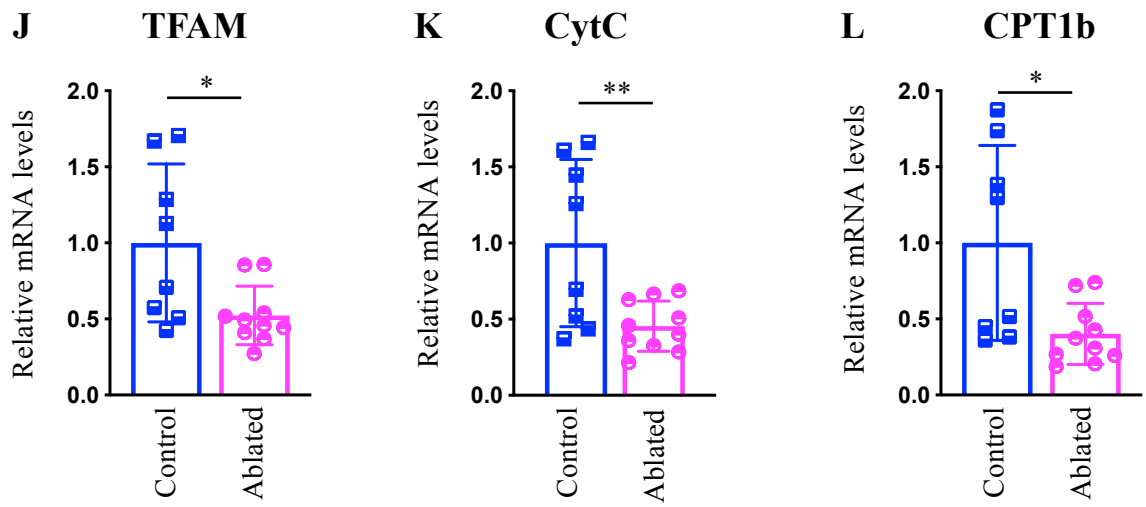

Figure 8: Effects of SF1 neuron ablation on genes expression in BAT of DIO mice.

Relative mRNA abundances of macrophage markers [F4/80 (A), CD11c (B), and CD206 (C)], inflammatory cytokines [TNF-α (D), IL-6 (E), and MCP-1 (F)], thermogenesis-related genes [UCP1 (G), PGC-1α (H), and DIO2 (I)], and mitochondrial genes [mitochondrial transcriptional factor A (TFAM) (J), cytochrome C (CytC) (K), and CPT1b (L)] in BAT of control and SF1-ablated mice. Mice were fed with HFD for 8 weeks as shown in the text and Figure 2. n=8 for control and n=10 for SF1-ablated mice. All data are shown in ± SD. *P < 0.05, **P < 0.01, unpaired *t*-test. Scatter plots display the data for individual mice. Ablated, SF1-ablated mice; Control, WT control mice.

Figure 9

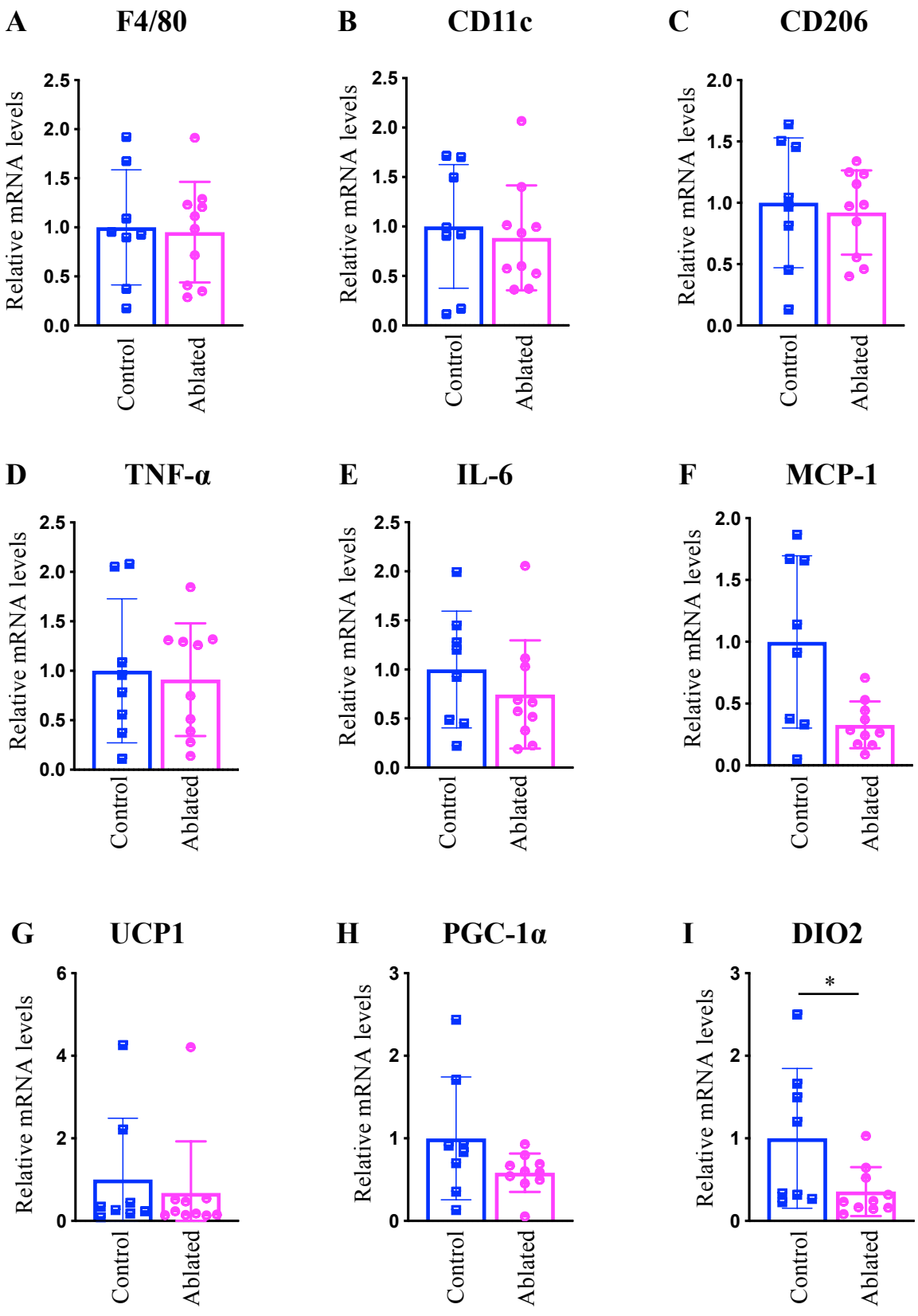
A
F4/80
B
CD11c
C
CD206
D
TNF-α
E
IL-6
F
MCP-1
G
UCP1
H
PGC-1α
I
DIO2
Relative mRNA levels
Control
Ablated
*

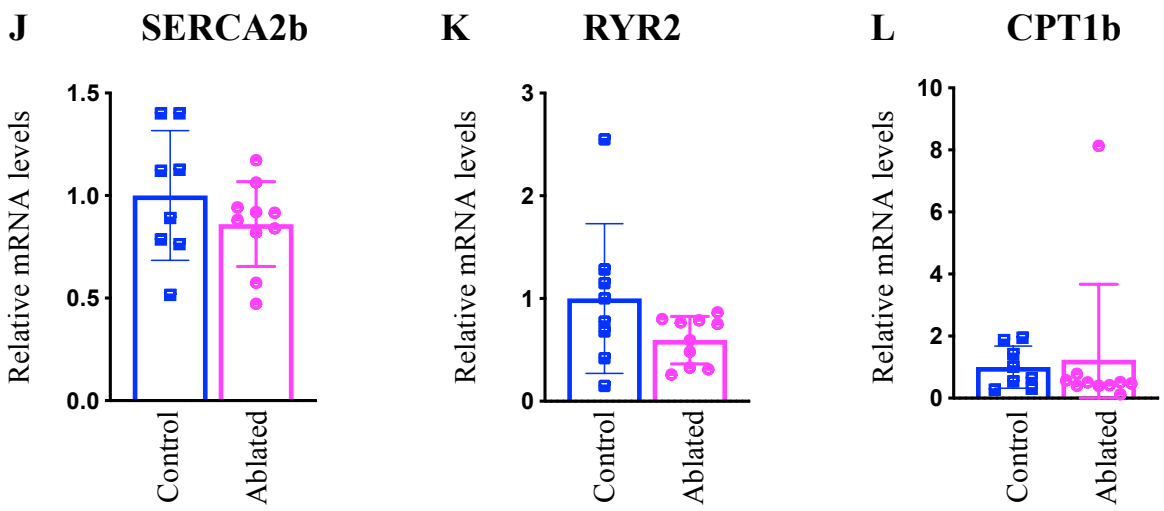

Figure 9: Effects of SF1 neuron ablation on genes expression in epiWAT of DIO mice.

Relative mRNA abundances of macrophage markers [F4/80 (A), CD11c (B), and CD206 (C)], inflammatory cytokines [TNF-α (D), IL-6 (E), and MCP-1 (F)], thermogenesis-related genes [UCP1 (G), PGC-1α (H), and DIO2 (I)], and mitochondrial genes [SERCA2b (J), RYR2 (K), and CPT1b (L)] in epiWAT of control and SF1-ablated mice. Mice were fed with HFD for 8 weeks as shown in the text and Figure 2. n=8 for control and n=10 for SF1-ablated mice. All data are shown in mean ± SD. *$P < 0.05$, unpaired *t*-test. Scatter plots display the data for individual mice. Ablated, SF1-ablated mice; Control, WT control mice.

Figure 10

A

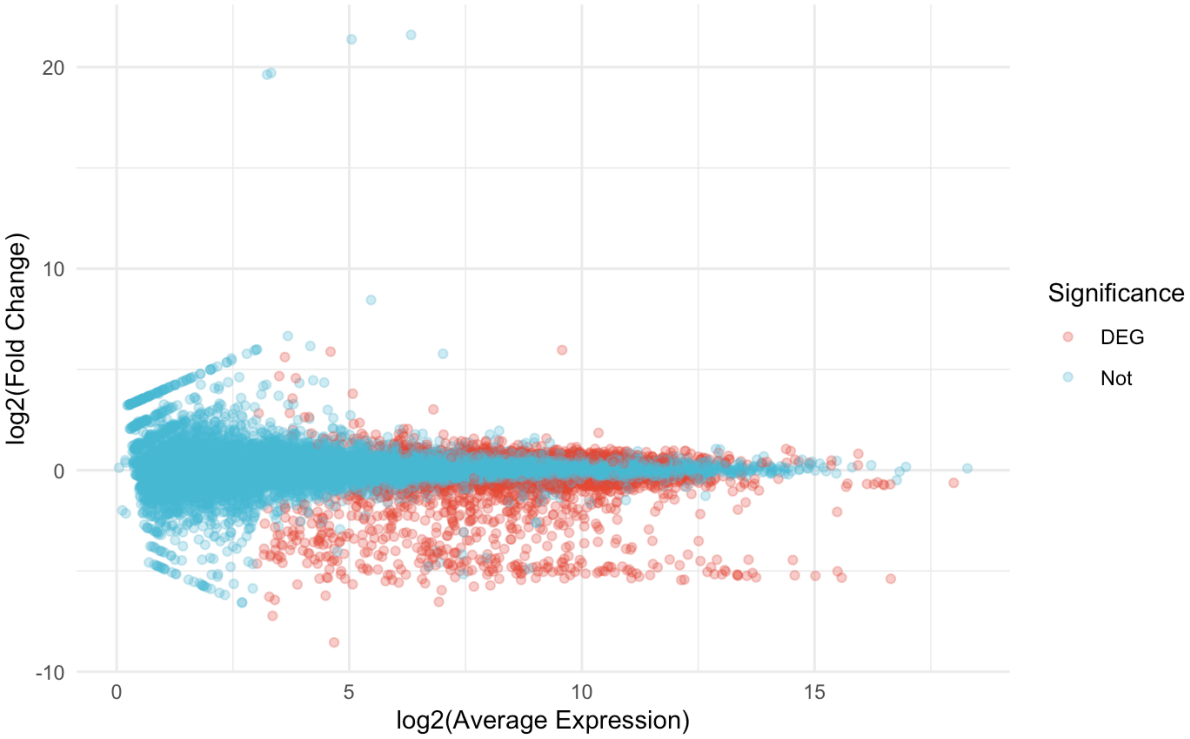
20
10
0
-10
log2(Fold Change)
0
5
10
15
log2(Average Expression)
Significance
DEG
Not

B

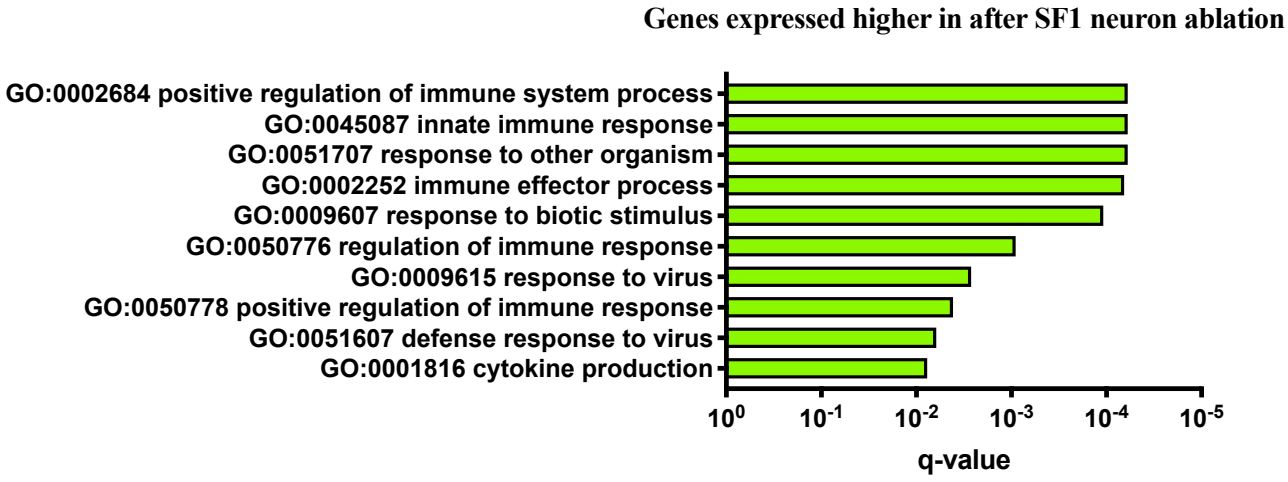
Genes expressed higher in after SF1 neuron ablation
GO:0002684 positive regulation of immune system process
GO:0045087 innate immune response
GO:0051707 response to other organism
GO:0002252 immune effector process
GO:0009607 response to biotic stimulus
GO:0050776 regulation of immune response
GO:0009615 response to virus
GO:0050778 positive regulation of immune response
GO:0051607 defense response to virus
GO:0001816 cytokine production
10^0
10^-1
10^-2
10^-3
10^-4
10^-5
q-value

C

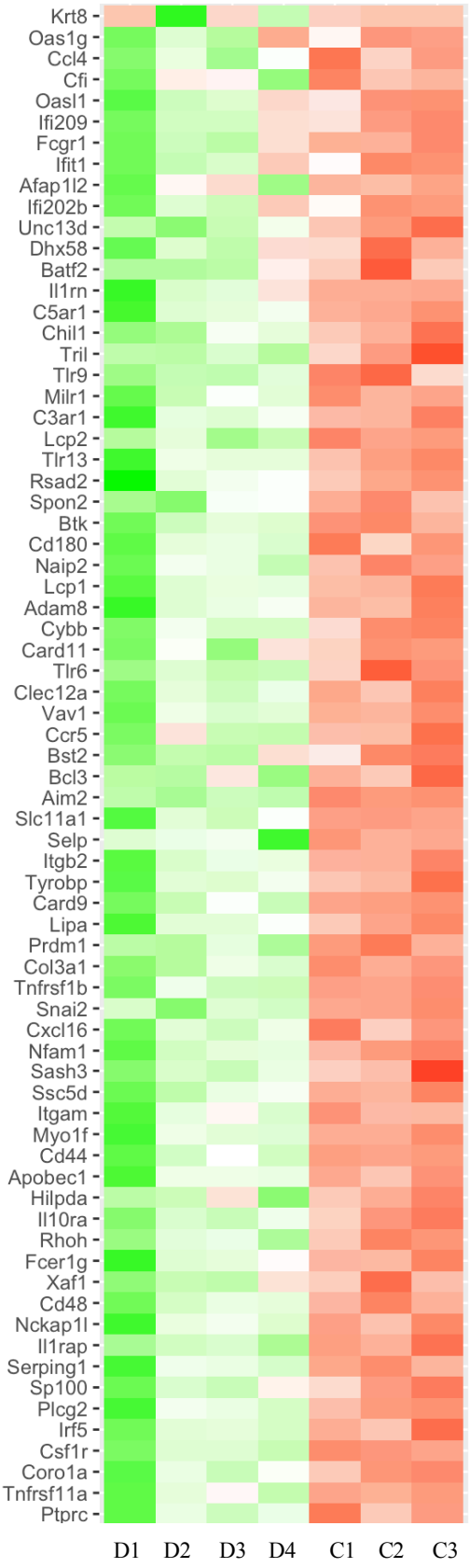
Krt8
Oas1g
Ccl4
Cfi
Oasl1
Ifi209
Fcgr1
Ifit1
Afap1l2
Ifi202b
Unc13d
Dhx58
Batf2
Il1rn
C5ar1
Chil1
Tril
Tlr9
Milr1
C3ar1
Lcp2
Tlr13
Rsad2
Spon2
Btk
Cd180
Naip2
Lcp1
Adam8
Cybb
Card11
Tlr6
Clec12a
Vav1
Ccr5
Bst2
Bcl3
Aim2
Slc11a1
Selp
Itgb2
Tyrobp
Card9
Lipa
Prdm1
Col3a1
Tnfrsf1b
Snai2
Cxcl16
Nfam1
Sash3
Ssc5d
Itgam
Myo1f
Cd44
Apobec1
Hilpda
Il10ra
Rhoh
Fcer1g
Xaf1
Cd48
Nckap1l
Il1rap
Serping1
Sp100
Plcg2
Irf5
Csf1r
Coro1a
Tnfrsf11a
Ptprc
D1
D2
D3
D4
C1
C2
C3

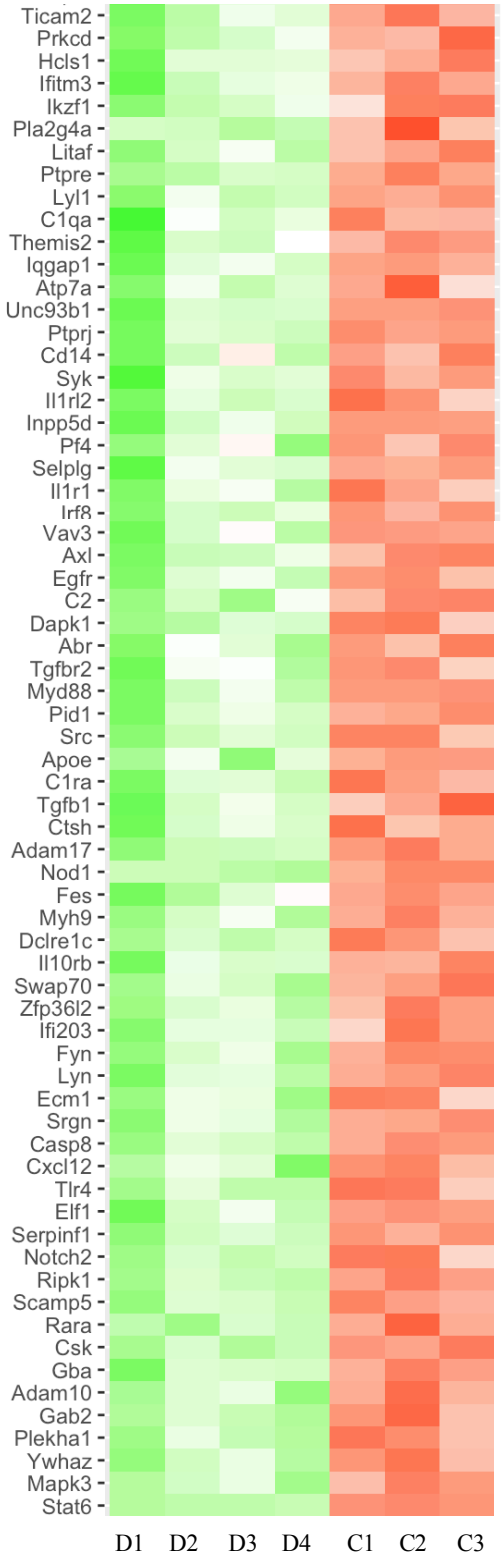
Ticam2
Prkcd
Hcls1
Ifitm3
Ikzf1
Pla2g4a
Litaf
Ptpre
Lyl1
C1qa
Themis2
Iqgap1
Atp7a
Unc93b1
Ptprj
Cd14
Syk
Il1rl2
Inpp5d
Pf4
Selplg
Il1r1
Irf8
Vav3
Axl
Egfr
C2
Dapk1
Abr
Tgfbr2
Myd88
Pid1
Src
Apoe
C1ra
Tgfb1
Ctsh
Adam17
Nod1
Fes
Myh9
Dclre1c
Il10rb
Swap70
Zfp36l2
Ifi203
Fyn
Lyn
Ecm1
Srgn
Casp8
Cxcl12
Tlr4
Elf1
Serpinf1
Notch2
Ripk1
Scamp5
Rara
Csk
Gba
Adam10
Gab2
Plekha1
Ywhaz
Mapk3
Stat6
D1
D2
D3
D4
C1
C2
C3

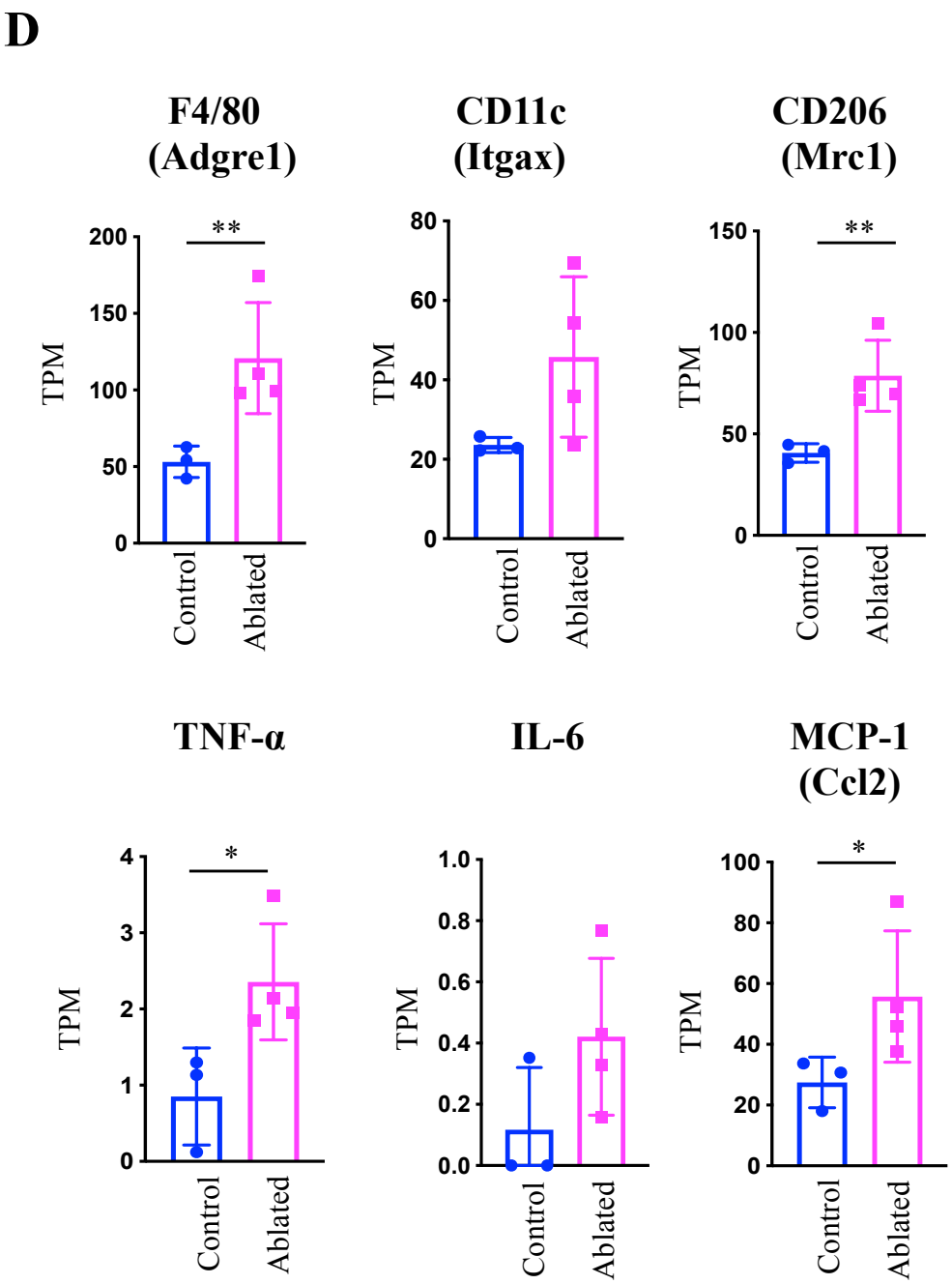

Figure 10: RNA-Seq analysis of ingWAT from the control and SF1-ablated mice.

(A) Plot depicting all detected genes with the average mRNA abundance and the fold expression in SF1 ablated mice when compared with the control mice. Red circles indicate genes that showed significant expression differences (differentially expressed genes, DEGs) ($P<0.05$, adjusted p-value) whereas blue circles indicate genes whose expression levels were

not significantly changed. (B) A list of top 10 gene ontologies most significantly enriched among DEGs expressed higher in ingWAT from SF1-ablated mice. (C) All individual mRNA abundances of DEGs expressed higher in ingWAT and annotated with the gene ontologies correlated with inflammatory responses. Individual gene ontologies used in this analysis are described in the method section. The heat map shows the relative mRNA abundances of individual samples compared with the averages of all samples (D1-D4; SF1-ablated animals, C1-C3; control animals). (D) RNA-Seq analysis confirmed the results of qPCR in Figure 6 for the mRNA abundances of macrophage markers (F4/80, CD11c, and CD206) and inflammatory cytokines (TNF-α, IL-6, and MCP-1) in SF1-ablated and control mice. Expression levels are indicated by transcripts per million (TPM). Mice were fed with HFD for 8 weeks as shown in the text and Figure 2. n=3 for control and n=4 for SF1-ablated mice. The results in (D) are shown in mean ± SD. *$P < 0.05$, unpaired t-test after log conversion. Scatter plots display the data for individual mice. Ablated, SF1-ablated mice; Control, WT control mice.

Figure 11

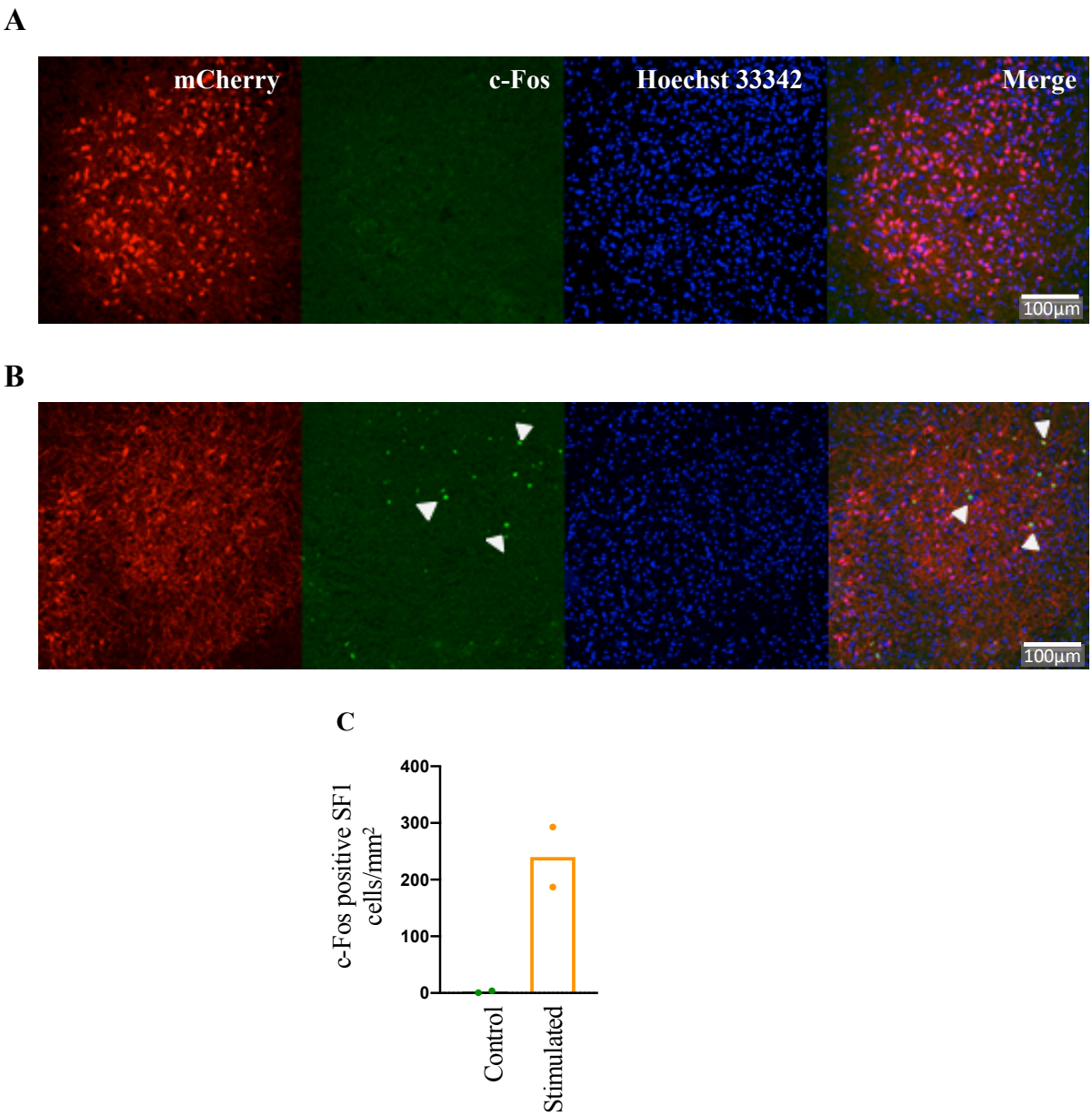

Figure 11: SF1 neuron activation in the VMH by DREADD technology.

(A, B) Adeno-associated viruses that express mCherry (A) or mCherry-fused hM3Dq (hM3Dq-mCherry) (B) in a Cre-recombinase-dependent manner were injected into the vicinity of the VMH area of SF1-Cre mice. Those mice were fed with ND for ~4 weeks and then provided CNO in drinking water for 1 day. Brain sections were immunostained for mCherry (red) and c-Fos (green). Sections were counterstained with Hoechst33342 (blue) for nuclear staining.

Arrowheads are indicating double-positive cells in the merged image that are c-Fos positive activated SF1 cells in the VMH. (C) Scatter plot shows the number of c-Fos positive cells per square millimeter of the VMH in mCherry (control) (n=2) and hM3Dq-mCherry (Stimulated) (n=2) expressing mice.

Figure 12

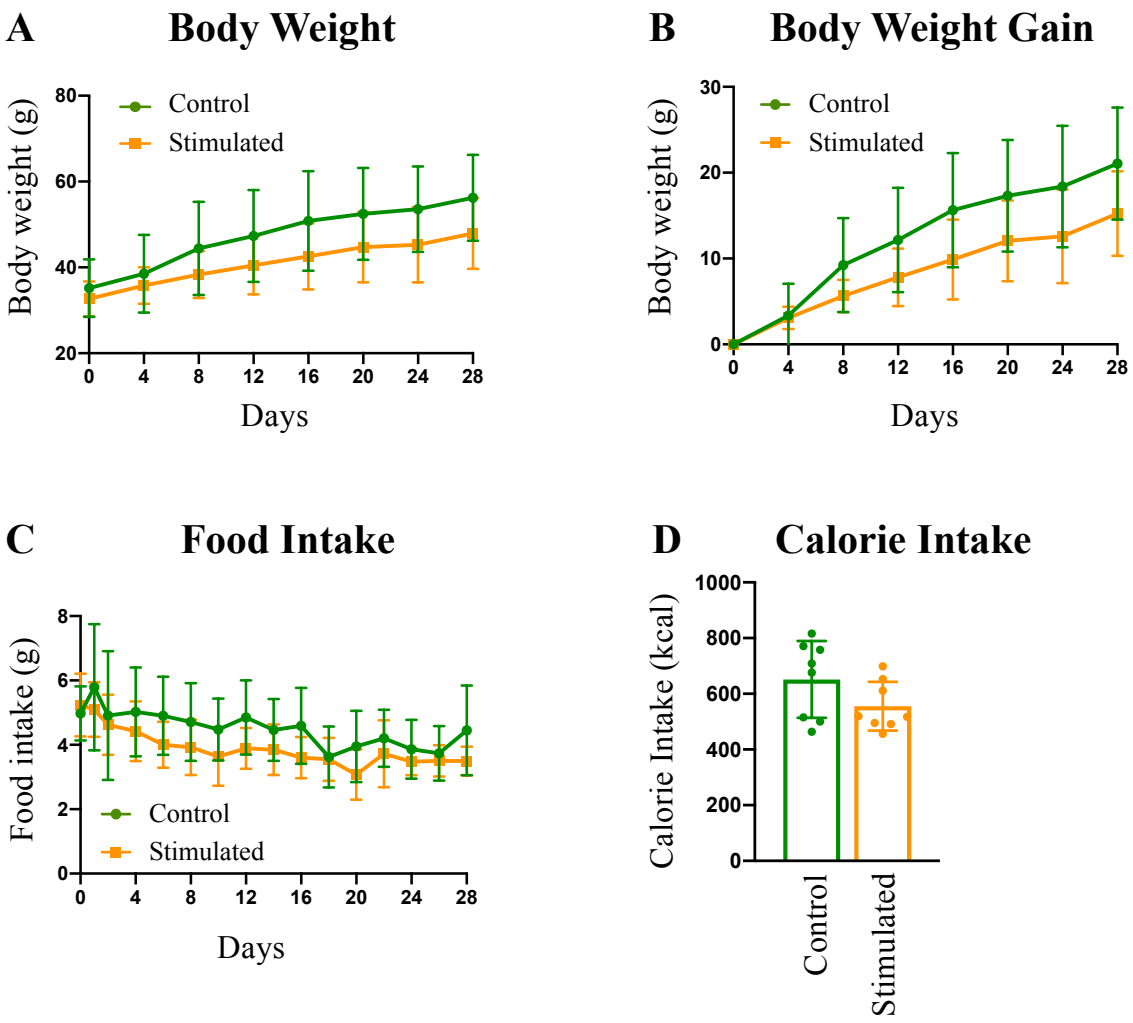

Figure 12: Effects of SF1 neuron activation on HFD-induced body weight increase and food intake.

(A, B) Body weight (A) and body weight gain (B) of the control and SF1-stimulated mice. HFD feeding and CNO administration started at Day 0. (C) Daily food intake during the HFD feeding period. (D) Total calorie intake during HFD feeding period. n=8 for each group. All data are shown in mean ± SD. Data were analyzed with a two-way ANOVA (A-C) or unpaired t-test (D). Scatter plot in (D) displays the data for individual mice. Stimulated, SF1-stimulated mice; Control, control mice.

Figure 13

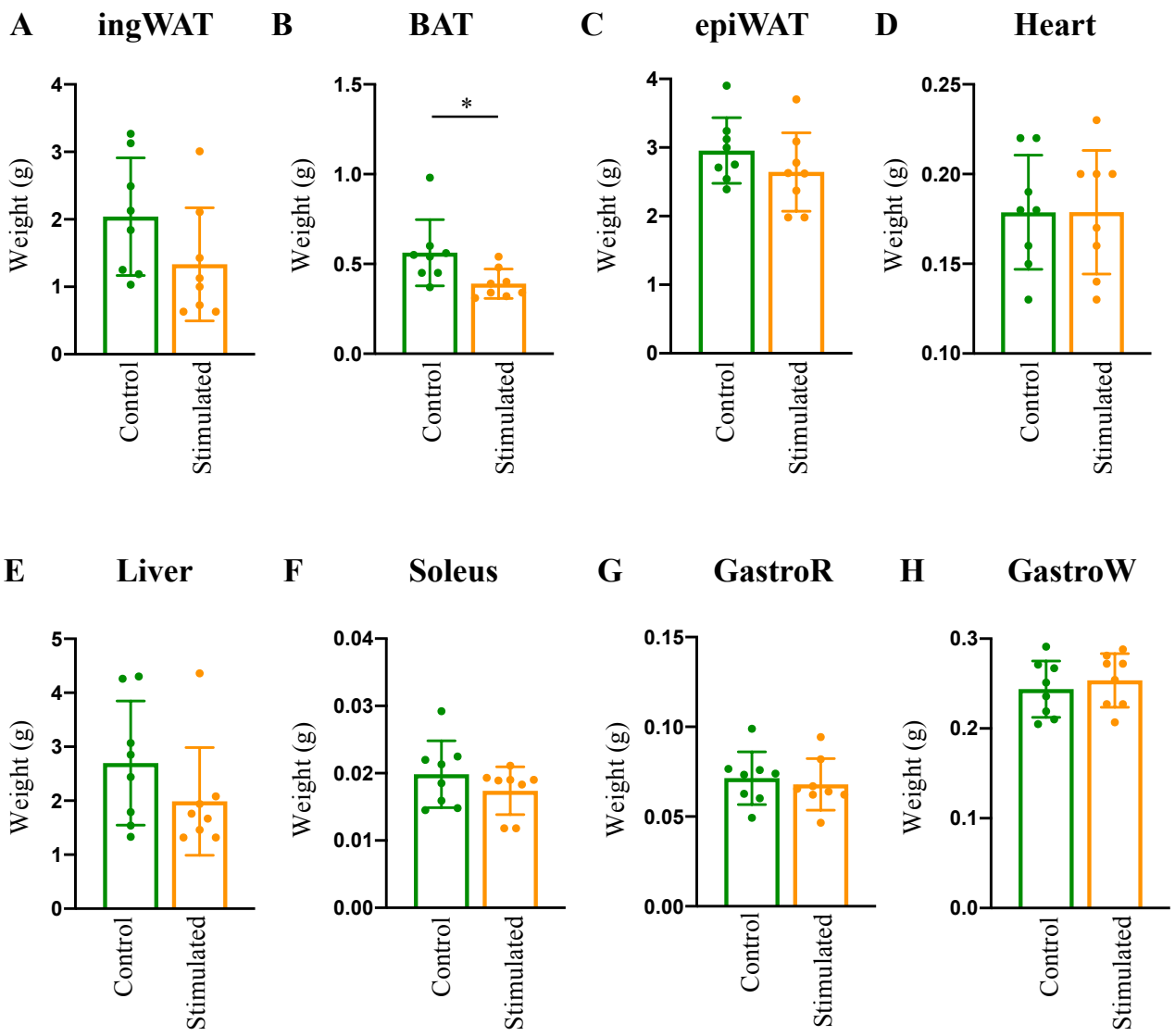

Figure 13: Effects of SF1 neuron activation on tissue weight of HFD-fed mice.

Tissue weights of ingWAT (A), BAT (B), epiWAT (C), heart (D), liver (E), three regions of skeletal muscles [soleus (F), GastroR (G), and GastroW (H)] of control and SF1-stimulated mice. Mice were fed with HFD for 4 weeks along with CNO administration in drinking water. n=8 for each group. All data are shown in mean ± SD. *P < 0.05, unpaired *t*-test. Scatter plots display the data for individual mice. Stimulated, SF1-stimulated mice; Control, control mice.

Figure 14

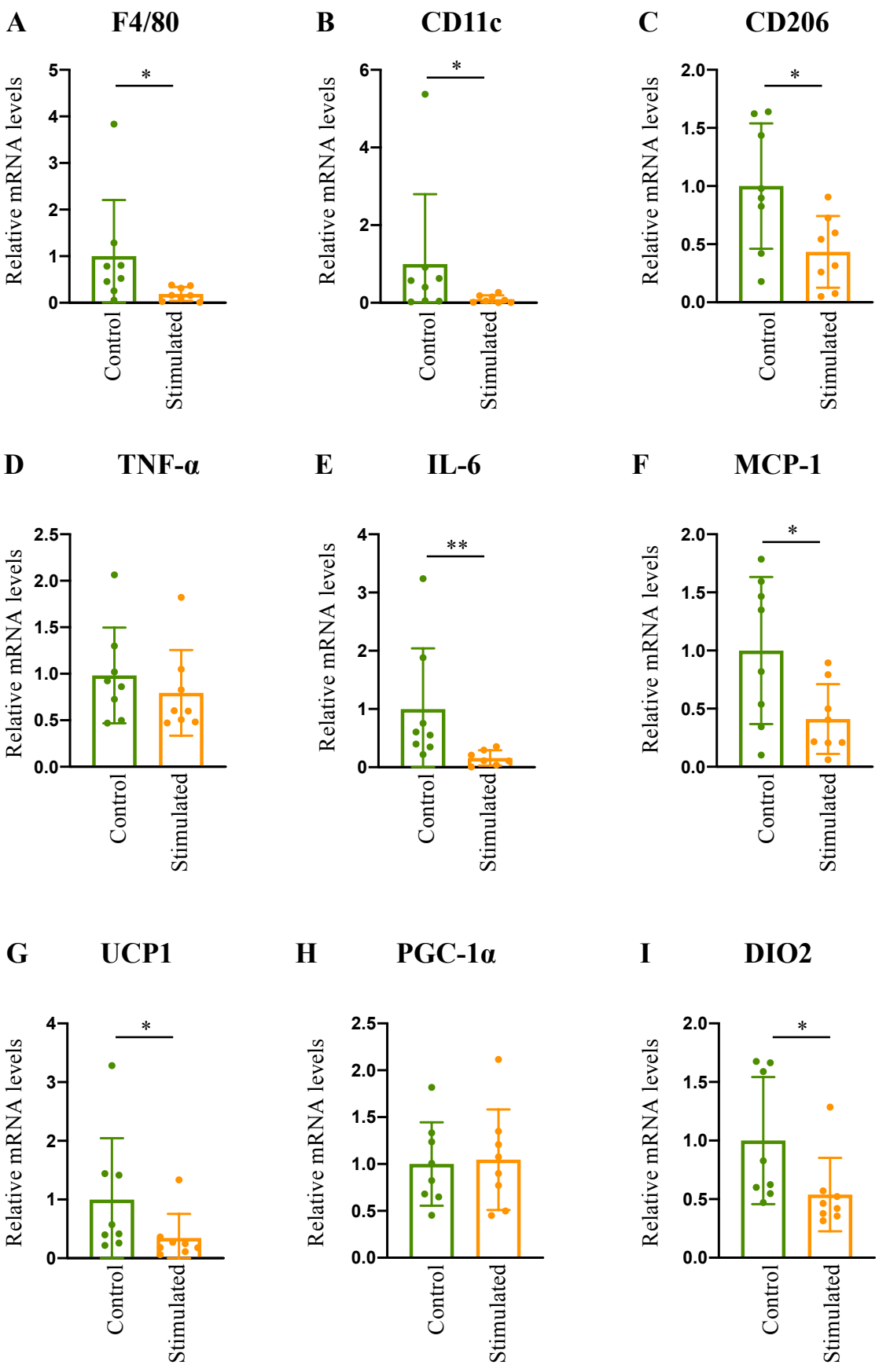
A
F4/80
B
CD11c
C
CD206
D
TNF-α
E
IL-6
F
MCP-1
G
UCP1
H
PGC-1α
I
DIO2
Relative mRNA levels
Control
Stimulated
*
**

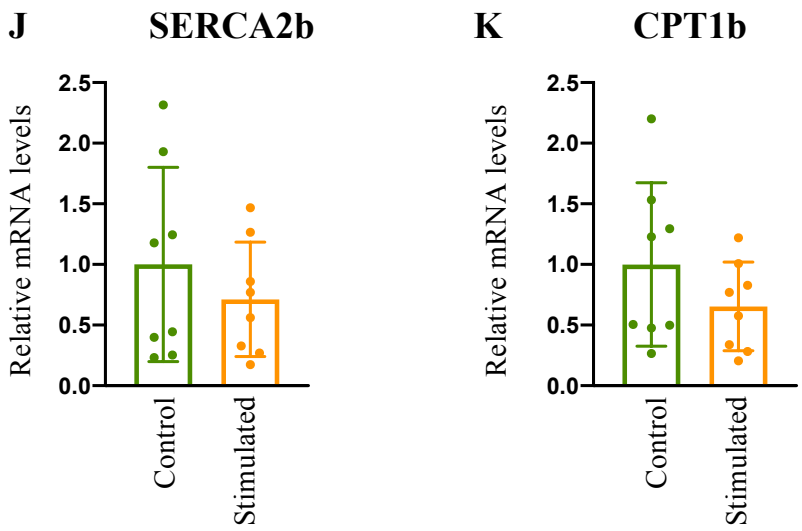

Figure 14: Genes expression affected by SF1 neuron activation during HFD feeding in ingWAT.

Relative mRNA abundances in ingWAT of mice expressing mCherry (Control) or hM3Dq-mCherry (Stimulated) in SF1 neurons, fed with HFD and administered CNO. Bar graphs show relative mRNA abundances for macrophage markers [F4/80 (A), CD11c (B), and CD206 (C)], inflammatory cytokines [TNF-α (D), IL-6 (E), and MCP-1 (F)], thermogenesis-related genes [UCP1 (G), PGC-1α (H), and DIO2 (I)], and mitochondrial genes [SERCA2b (J) and CPT1b (K)] in control and SF1-stimulated mice. n=8 for each group. All data are shown in mean ± SD. *P < 0.05, **P<0.01 unpaired *t*-test. Scatter plots display the data for individual mice. Stimulated, SF1-stimulated mice; Control, control mice.

Figure 15

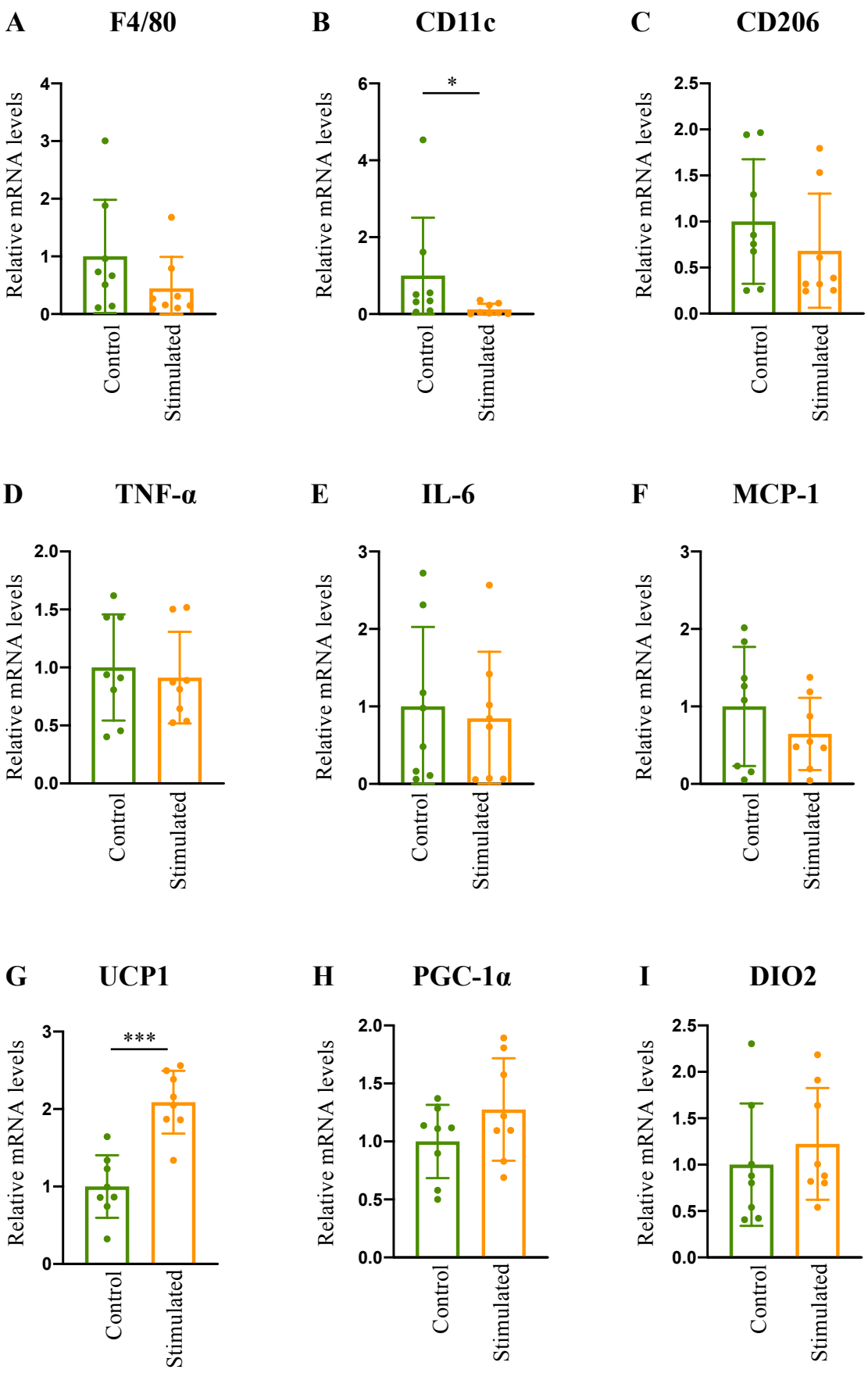
A
F4/80
B
CD11c
C
CD206
D
TNF-α
E
IL-6
F
MCP-1
G
UCP1
H
PGC-1α
I
DIO2
Relative mRNA levels
Control
Stimulated
*
***

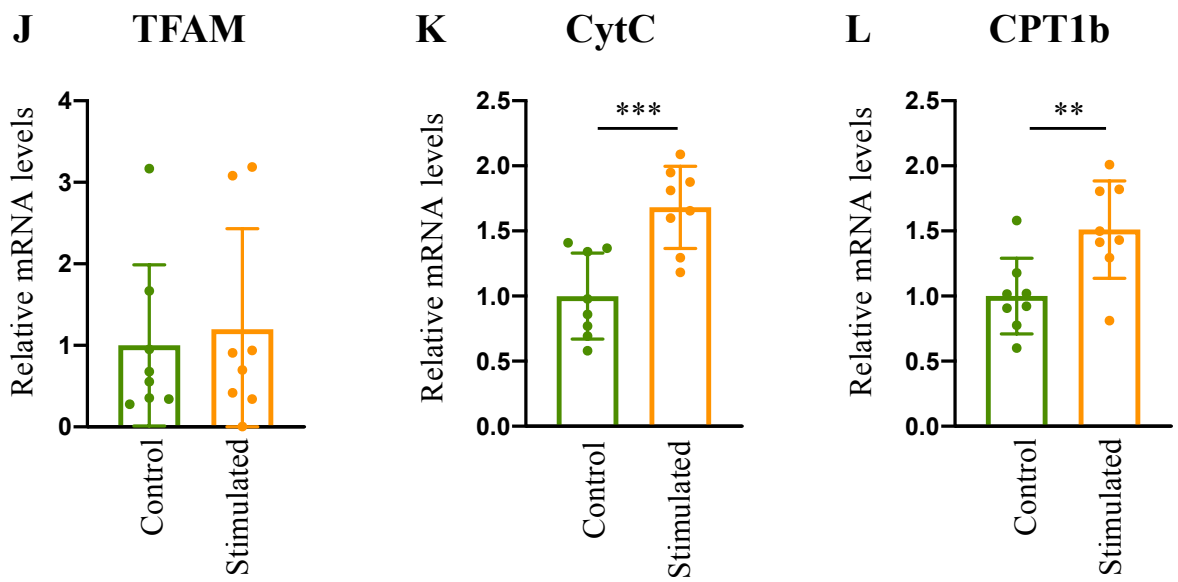

Figure 15: Genes expression affected by SF1 neuron activation during HFD feeding in BAT.

Relative mRNA abundances in BAT of mice expressing mCherry (Control) or hM3Dq-mCherry (Stimulated) in SF1 neurons, fed with HFD and administered CNO. Bar graphs show relative mRNA abundances for macrophage markers [F4/80 (A), CD11c (B), and CD206 (C)], inflammatory cytokines [TNF-α (D), IL-6 (E), and MCP-1 (F)], thermogenesis-related genes [UCP1 (G), PGC-1α (H), and DIO2 (I)], and mitochondrial genes [TFAM)(J), CytC (K), and CPT1b (L)] in control and SF1-stimulated mice. n=8 for each group. All data are shown in mean ± SD. *P < 0.05, **P < 0.01, ***P < 0.001, unpaired *t*-test. Scatter plots display the data for individual mice. Stimulated, SF1-stimulated mice; Control, control mice.

Figure 16

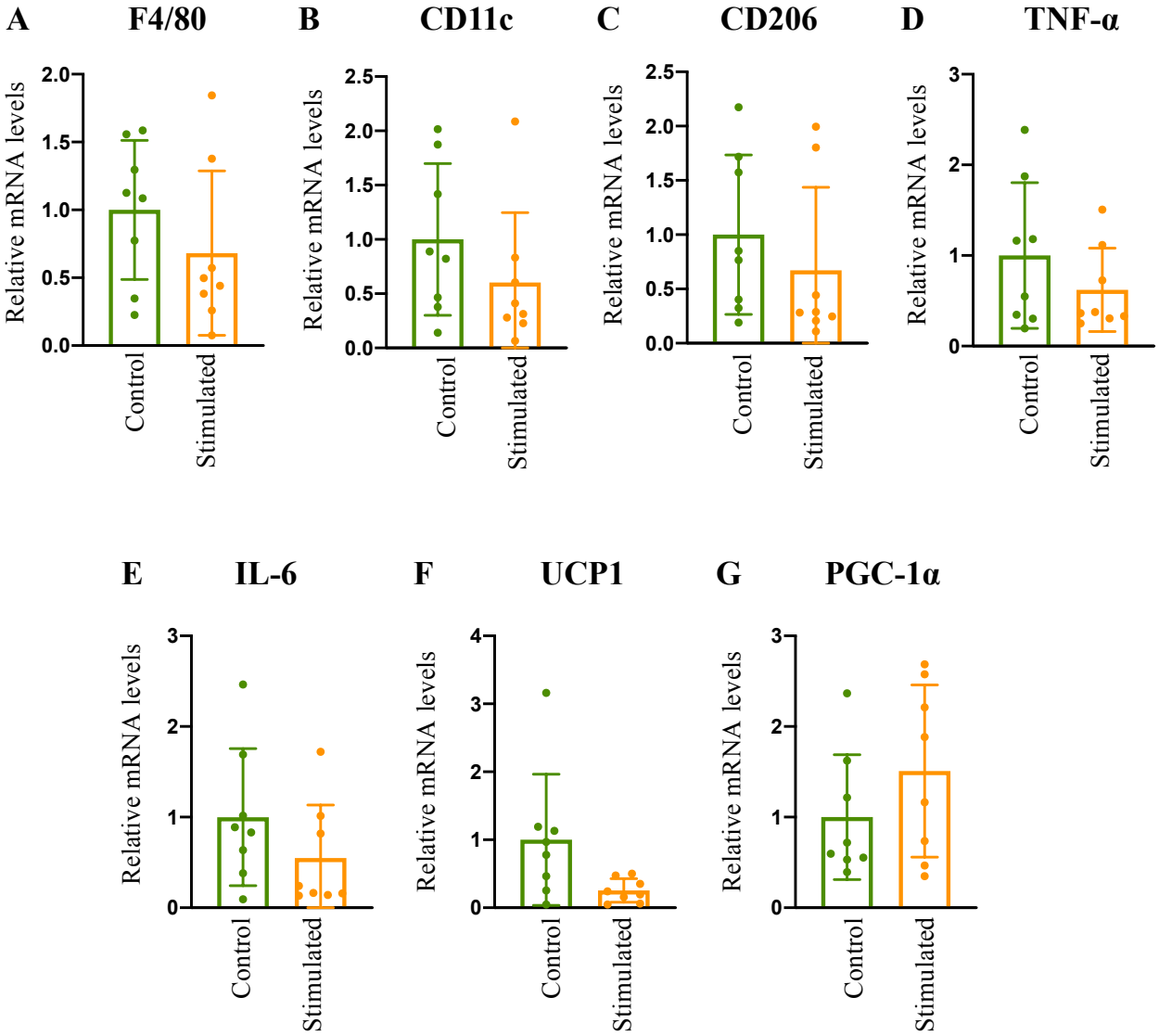

Figure 16: Genes expression affected by SF1 neuron activation during HFD feeding in epiWAT.

Relative mRNA abundances in epiWAT of mice expressing mCherry (Control) or hM3Dq-mCherry (Stimulated) in SF1 neurons, fed with HFD and administered CNO. Bar graphs show relative mRNA levels for macrophage marker [F4/80 (A), CD11c (B), and CD206 (C)], inflammatory cytokines [TNF-α (D) and IL-6 (E)], and thermogenesis-related genes [UCP1 (F) and PGC-1α (G)] in control and SF1-stimulated mice. n=8 for each group. All data are

shown in mean ± SD. Scatter plots display the data for individual mice. Stimulated, SF1-stimulated mice; Control, control mice.

Figure 17

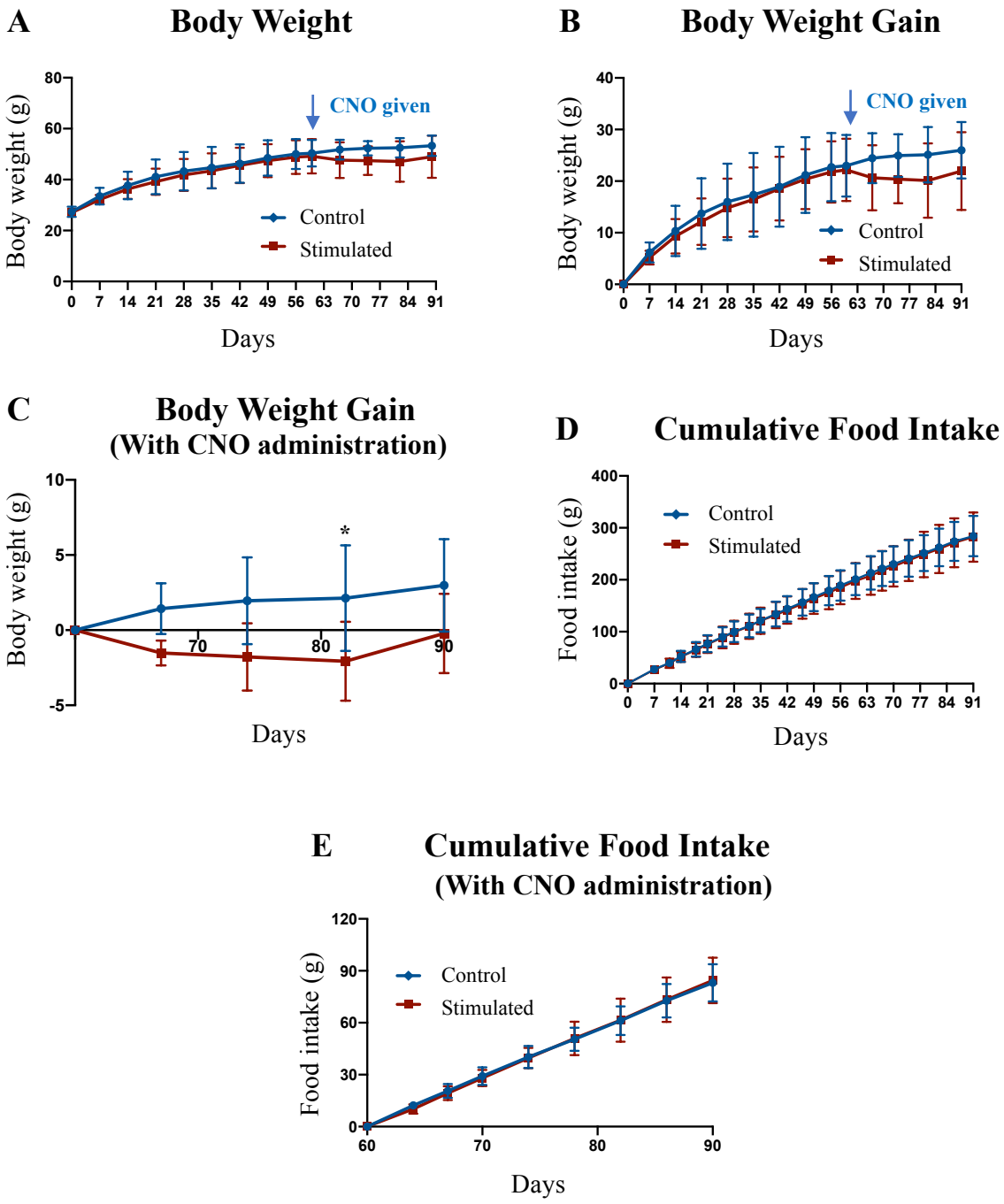

Figure 17: Effects of chronic activation of SF1 neurons on body weight and food intake of DIO mice.

(A - C) Body weight (A) and body weight gain (B) throughout HFD fed period, and body weight gain (C) during CNO administration period. HFD was fed from Day 0, and CNO

administration was started at Day 60 (indicated by arrows). (D, E) Cumulative food intake throughout the HFD fed period (D) and during the CNO administration period (E). n=6 for control mice, n=5 for stimulated mice. All data are shown in ± SD. *$P < 0.05$, two-way ANOVA with post-hoc Sidak's test. Stimulated, SF1-stimulated mice; Control, control mice.

Figure 18

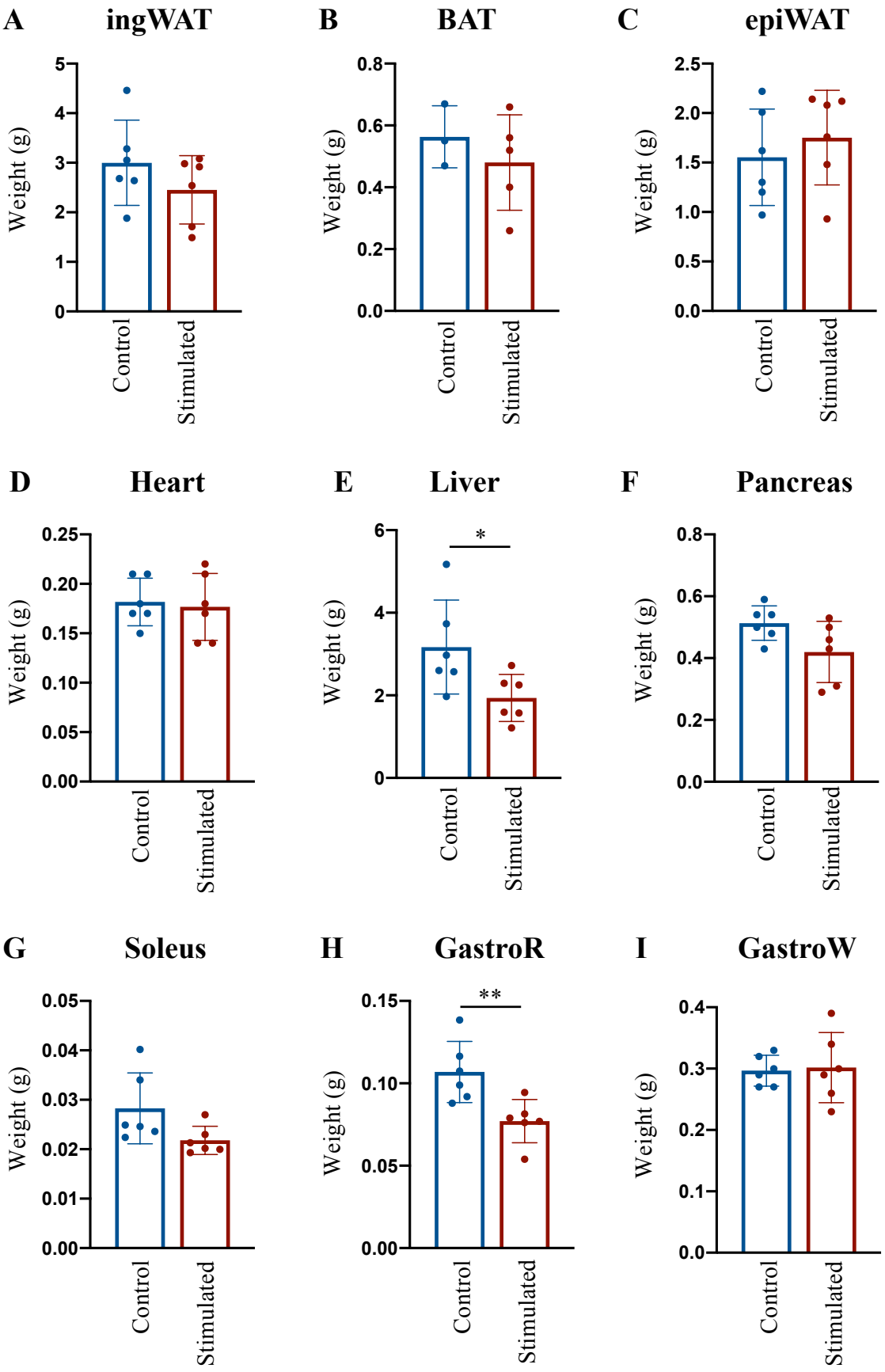
A
ingWAT
Weight (g)
5
4
3
2
1
0
Control
Stimulated
B
BAT
Weight (g)
0.8
0.6
0.4
0.2
0.0
Control
Stimulated
C
epiWAT
Weight (g)
2.5
2.0
1.5
1.0
0.5
0.0
Control
Stimulated
D
Heart
Weight (g)
0.25
0.20
0.15
0.10
0.05
0.00
Control
Stimulated
E
Liver
*
Weight (g)
6
4
2
0
Control
Stimulated
F
Pancreas
Weight (g)
0.8
0.6
0.4
0.2
0.0
Control
Stimulated
G
Soleus
Weight (g)
0.05
0.04
0.03
0.02
0.01
0.00
Control
Stimulated
H
GastroR
**
Weight (g)
0.15
0.10
0.05
0.00
Control
Stimulated
I
GastroW
Weight (g)
0.4
0.3
0.2
0.1
0.0
Control
Stimulated

Figure 18: Effects of chronic activation of SF1 neurons on tissue weights of DIO mice.

Tissue weights of ingWAT (A), BAT (B), epiWAT (C), heart (D), liver (E), pancreas (F), and three regions of skeletal muscles [soleus (G), GastroR (H), and GastroW (I)] of control and SF1-stimulated mice. Mice were fed with HFD for 8 weeks before CNO administration and continued HFD feeding during 4 weeks of CNO administration as shown in the text and Figure 17. n=6 for each group except BAT (n=3 control, n=5 stimulated) All data are shown in mean ± SD. *$P < 0.05$, **$P < 0.01$, unpaired *t*-test. Scatter plots display the data for individual mice. Stimulated, SF1-stimulated mice; Control, control mice.

Figure 19

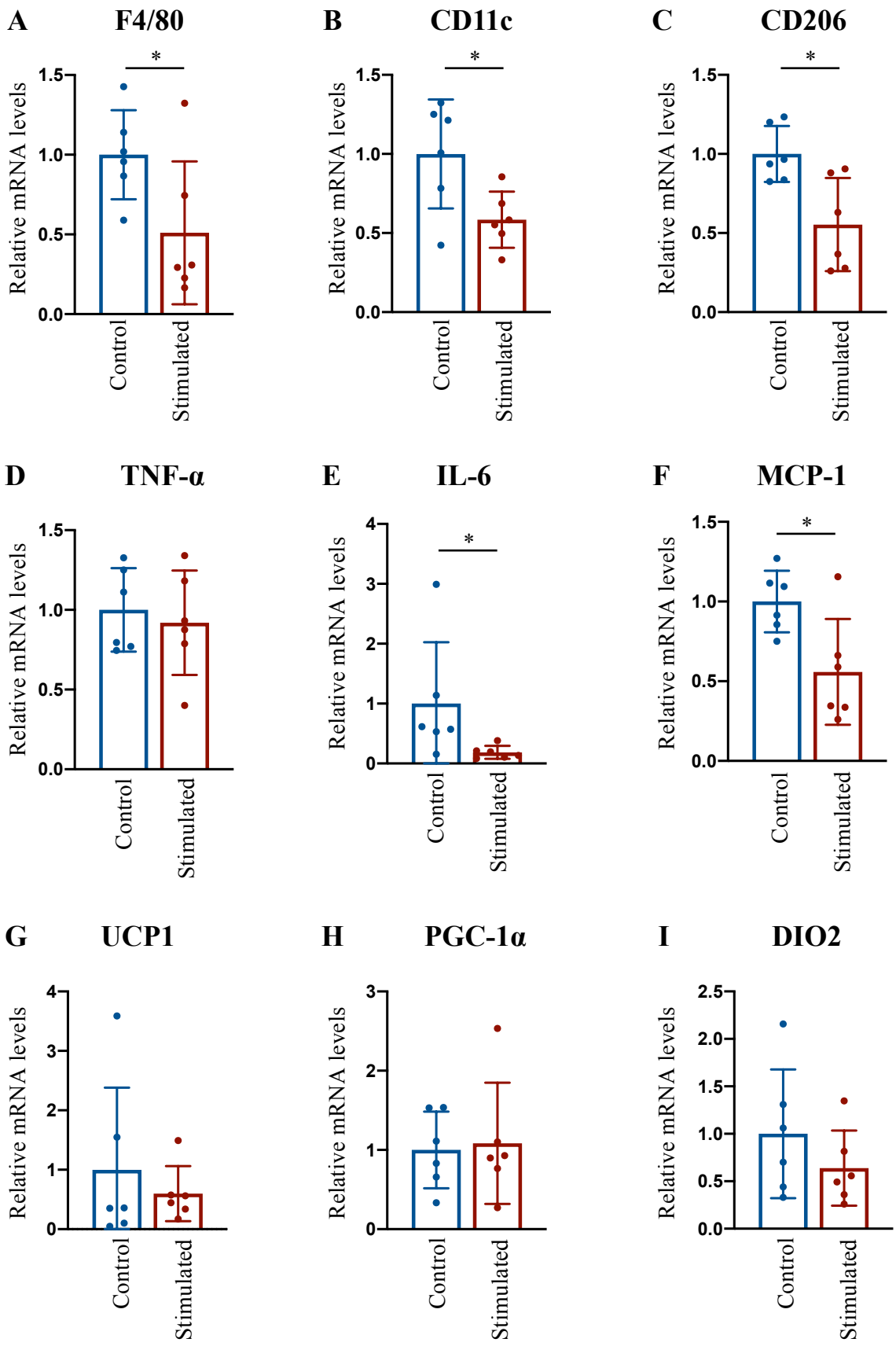
A
F4/80
B
CD11c
C
CD206
D
TNF-α
E
IL-6
F
MCP-1
G
UCP1
H
PGC-1α
I
DIO2
Relative mRNA levels
Control
Stimulated
*

Figure 19: Effects of chronic activation of SF1 neurons on genes expression in ingWAT of DIO mice.

Relative mRNA abundances of macrophage markers [F4/80 (A), CD11c (B), and CD206 (C)], inflammatory cytokines [TNF-α (D), IL-6 (E), and MCP-1 (F)], and thermogenesis-related genes [UCP1(G), PGC-1α (H), and DIO2 (I)] in ingWAT of control and SF1-stimulated mice. n=8 for each group. Mice were fed with HFD for 8 weeks before CNO administration and continued HFD feeding during 4 weeks of CNO administration as shown in the text and Figure 17. All data are shown in mean ± SD. *$P < 0.05$, unpaired *t*-test. Scatter plots display the data for individual mice. Stimulated, SF1-stimulated mice; Control, control mice.

Table 1: List of primers for RT-qPCR

Primer	Forward sequence	Reverse Sequence
36B4	GGCCCTGCACTCTCGCTTTC	TGCCAGGACGCGCTTGT
F4/80	CTTTGGCTATGGGCTTCCAGTC	GCAAGGAGGACAGAGTTTATCGTG
CD206	CAAGGAAGGTTGGCATTTGT	CCTTTCAGTCCTTTGCAAGC
CD11c	ATTTCTGAGAGCCCAGACGA	CCATTTGCTTCCTCCAACAT
TNF-α	ATCCGCGACGTGGAACTG	ACCGCCTGGAGTTCTGGAA
IL-6	ACAACCACGGCCTTCCCTACTT	CACGATTTCCCAGAGAACATGTG
MCP-1	CCACTCACCTGCTGCTACTCAT	TGGTGATCCTCTTGTAGCTCTCC
UCP1	GGCCCTTGTAAACAACAAAATAC	GGCAACAAGAGCTGACAGTAAAT
PGC-1α	AAGTGTGGAACTCTCTGGAACTG	GGGTTATCTTGGTTGGCTTTATG
DIO2	CAGTGTGGTGCACGTCTCCAATC	TGAACCAAAGTTGACCACCAG
TFAM	CCAAAAAGACCTCGTTCAGC	CTTCAGCCATCTGCTCTTCC
CytC	GGAGGCAAGCATAAGACTGG	TCCATCAGGGTATCCTCTCC
CPT1b	GTCGCTTCTTCAAGGTCTGG	AAGAAAGCAGCACGTTCGAT
SERCA2b	ACCTTTGCCGCTCATTTTCCAG	AGGCTGCACACACTCTTTACC
RYR2	ATGGCTTTAAGGCACAGCG	CAGAGCCCGAATCATCCAGC

Acknowledgments

My first gratitude is to Almighty ALLAH, who is kind and forgiving, Who has given us the ability to discover what He has created and Whose blessing and exaltations flourished my thoughts and enabled me to improve my knowledge up to this stage. I thank ALLAH that despite all problems, which I encountered during my Ph.D. enabled me to complete this dissertation. I offer my humble and sincerest words of thanks, to our beloved Holy Prophet, HAZRAT MUHAMMAD (PBUH) whose teachings guide us towards knowledge.

I would like to express my deep gratitude to my respected supervisor, Prof. Dr. Yasuhiko Minokoshi, for his guidance, enthusiastic encouragement, and useful critiques of this research work. I heartily appreciate and am greatly indebted to my assistant Prof. Dr. Kunio Kondoh, for his patience, continued guidance and, advice throughout the research development and analysis. It is a great pleasure penning my acknowledgment towards Prof. Dr. Yoshihiro Kubo and Prof. Dr. Makato Tominaga for their guidance, co-operation, and knowledgeable help during my Ph.D.

My grateful thanks are also extended to Prof. Dr. ken-Ichiro Nakajima and all other lab mates and friends especially May, for support and encouragement throughout my study. I would like to thank Dr. Tanaka san, my early lab friend who gave me lively company at the start of my career. Thank you so much for being kind and friendly to me. Special thanks to Dr. Gergo Palfalvi (National Institute for Basic Biology) for helping in RNA sequencing data analysis.

I am indeed humbly grateful to my family, the first community that encouraged me to find my passion in research. My greatest thanks to my beloved mother and my brothers for their support, prayers, and encouragement. I am greatly obliged and wish to extend my gratitude to my all sisters and friends in my homeland for their prayers and encouragement

during the tenure of the research work. I can never forget my beloved father (late) who gave me self-confidence to walk through thick and thin with courage. May his soul rest in peace (Ameen). I wish he could have seen me in the position he desired.

Words are lacking to express thanks to my best friend and beloved husband for his company, endearment, care, support, co-operation, and consolatory behavior throughout my research work.

Finally, I would like to thank everybody who helps me morally to the successful completion of my thesis.